

pubs.acs.org/JCTC Review

Algebraic Diagrammatic Construction Theory for Simulating Charged Excited States and Photoelectron Spectra

Samragni Banerjee and Alexander Yu. Sokolov*



Cite This: J. Chem. Theory Comput. 2023, 19, 3037-3053

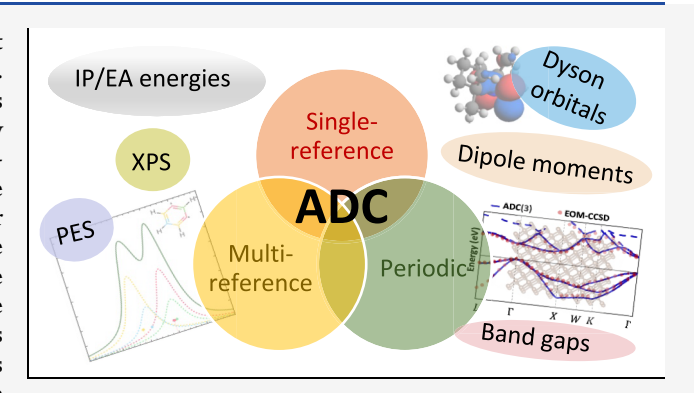


ACCESS I

III Metrics & More

Article Recommendations

ABSTRACT: Charged excitations are electronic transitions that involve a change in the total charge of a molecule or material. Understanding the properties and reactivity of charged species requires insights from theoretical calculations that can accurately describe orbital relaxation and electron correlation effects in openshell electronic states. In this Review, we describe the current state of algebraic diagrammatic construction (ADC) theory for simulating charged excitations and its recent developments. We start with a short overview of ADC formalism for the one-particle Green's function, including its single- and multireference formulations and extension to periodic systems. Next, we focus on the capabilities of ADC methods and discuss recent findings about their accuracy for calculating a wide range of excited-state



properties. We conclude our Review by outlining possible directions for future developments of this theoretical approach.

1. INTRODUCTION

Electronic excitations that change the charge state of molecules or materials are central to many important processes in chemistry, biochemistry, and materials science. Playing a crucial role in redox chemistry and catalysis, charged excitations are also common in atmospheric and combustion chemical reactions and are responsible for structural damage in some biomolecules. Additionally, charged excitations are the primary transitions probed by photoelectron spectroscopy, which reveals important details about the electronic structure of molecules and materials by measuring the binding energies of core and valence electrons. Charged electronic states can be accessed via chemical oxidation or reduction, photoexcitation, or direct electron attachment or ionization in the gas phase or electrochemical cell.

Theoretical simulations are essential for investigating the electronic structure and properties of charged excited states, which are often elusive and difficult to study experimentally. However, simulating charged excitations presents many challenges that put stringent requirements on what kind of theoretical methods can deliver accurate energies and properties of charged excited states. Changing the charge state of a molecule or material significantly perturbs their electronic density, altering the size of orbitals and the distribution of charge carriers. To accurately model these effects, it is necessary to use advanced theoretical techniques that take into account orbital relaxation and electron correlation in open-shell states with complex electronic structures.

Theoretical methods for simulating charged excitations can be divided into two broad categories: (i) the energy difference (or Δ) approaches and (ii) the direct (or response) theories. The Δ methods^{23–39} compute charged excitation energies and properties by performing separate calculations for each electronic state, including the neutral ground state. These simulations typically begin with a self-consistent-field $(\Delta SCF)^{23-28,40,41}$ or complete-active-space SCF $(\Delta CASSCF)^{25,29}$ optimization of electronic wave function, followed by a post-ΔSCF or post-ΔCASSCF treatment of dynamic electron correlation. 42,43 Although the Δ approaches can accurately capture relaxation of orbitals and wave functions upon charged excitation, their computations are only straightforward for the lowest-energy excited states of particular symmetry. For the higher-energy excited states, the Δ SCF or Δ CASSCF wave function optimizations are prone to convergence problems or variational collapse to lower-energy states. In addition, the wave functions calculated using the Δ methods may not be orthogonal to each other, and their calculations become prohibitively expensive for systems with high density of states.

Received: March 5, 2023 Published: May 16, 2023





In contrast to the Δ methods, response theories perform a single calculation for all electronic states simultaneously, ensuring that their wave functions are orthogonal. These methods optimize the ground-state wave function and compute the excitation energies and transition properties by assuming that the electron correlation in all states (ground and excited) is similar. Although response theories are less powerful than the Δ methods in capturing the wave function relaxation effects, their calculations are more efficient, do not suffer from systematic convergence problems, and can yield accurate results provided that they employ a sufficiently high level of electron correlation treatment. For these reasons, a wide range of response methods have been developed, including time-dependent density functional theory, 44-48 propagator (or Green's function) approaches, 49-58 traditional and symmetry-adapted-cluster configuration interaction, ^{59–66} and coupled cluster theory (CC) in linear-response ^{67–71} or equation-of-motion ^{72–79} formulations.

A special class of response methods is algebraic diagrammatic construction (ADC) theory.^{80–87} Since its original formulation in 1982 by Jochen Schirmer, ADC has become one of the standard electronic structure theories for simulating neutral excited states and UV/vis spectra of molecules, owing to the moderate computational cost and relatively high accuracy of its methods. Although traditionally formulated within the propagator formalism, conventional (singlereference) ADC theory has a close connection with wave function-based Møller-Plesset perturbation theory88 and equation-of-motion CC (EOM-CC), 72-79 offering a hierarchy of size-consistent methods that systematically improve accuracy with increasing order of approximation. Taking advantage of noniterative and Hermitian equations, low-order ADC methods are more computationally efficient than EOM-CC with single and double excitations (EOM-CCSD) and are capable of delivering results with similar accuracy. In addition to neutral excited states, the ADC framework has been extended to simulating charged and two-photon electronic transitions with excitation energies spanning from the visible to X-ray regions of the electromagnetic spectrum. 81,89-10

The original formulation of ADC methods for charged excitations proposed in 1983 was based on the Dyson ADC framework, 81 which allows one to simulate the electronattached (N + 1) and ionized (N - 1) states in one calculation by approximately solving the Dyson equation. In 1998, Schirmer, Trofimov, and Stelter formulated the non-Dyson ADC formalism⁹⁰ that enables one to calculate the N + 1 or N- 1 excited states independently from each other, bypassing the solution of the Dyson equation in a manner similar to Green's function methods based on coupled cluster theory^{72-74,109-111} developed earlier. Although the non-Dyson ADC methods are more computationally efficient than those based on the Dyson ADC framework, the number of studies reporting their calculations remained small until 2019 when these methods received a renewed interest. 96-102

In this Review, we describe the current state of non-Dyson ADC theory for charged excitations, including the recent progress in single-reference ADC for molecules and periodic materials, and the development of multireference ADC for molecular systems with challenging electronic structure. We begin with a brief overview of theoretical background behind ADC and its approximations (Section 2). We then discuss the capabilities of ADC methods and summarize recent findings about their accuracy (Section 3). Finally, we conclude our

Review by discussing possible directions for future developments (Section 4).

2. THEORETICAL BACKGROUND

2.1. One-Particle Green's Function. The central mathematical object in the ADC theory of charged excitations is the one-particle Green's function (or so-called single-particle propagator, 1-GF), which for an N-electron chemical system contains information about the energies and properties of all electron-attached (N+1) and ionized (N-1) states. 112-114 1-GF can be expressed as an expectation value

$$G_{pq}(t, t') = -i \langle \Psi_0^N | \mathcal{T}[a_p(t) a_q^{\dagger}(t')] | \Psi_0^N \rangle$$
(1)

where $|\Psi_0^N\rangle$ is the *N*-electron ground-state wave function, $a_q^\dagger(t')$ is a creation operator that adds an electron to spin—orbital $|\psi_q\rangle$ at time t', $a_p(t)$ is an annihilation operator that removes an electron from spin—orbital $|\psi_p\rangle$ at a different time t, and $\mathcal T$ is the operator responsible for time-ordering. Equation 1 describes both the forward (t>t') and backward (t<t') processes in time corresponding to the one-electron attachment and ionization of the ground electronic state, respectively.

By carrying out a Fourier transformation of eq 1, the 1-GF can also be defined in the frequency domain as

$$G_{pq}(\omega) = \langle \Psi_0^N | a_p (\omega - H + E_0^N)^{-1} a_q^{\dagger} | \Psi_0^N \rangle$$

$$+ \langle \Psi_0^N | a_q^{\dagger} (\omega + H - E_0^N)^{-1} a_p | \Psi_0^N \rangle$$
(2)

where H is the electronic Hamiltonian, E_0^N is the ground-state energy, and ω is the frequency of incident radiation. Alternatively, the frequency-dependent 1-GF can be expressed in the spectral (or Lehmann) representation 115

$$G_{pq}(\omega) = \sum_{n} \frac{\langle \Psi_{0}^{N} | a_{p} | \Psi_{n}^{N+1} \rangle \langle \Psi_{n}^{N+1} | a_{q}^{\dagger} | \Psi_{0}^{N} \rangle}{\omega - E_{n}^{N+1} + E_{0}^{N}}$$

$$+ \sum_{n} \frac{\langle \Psi_{0}^{N} | a_{q}^{\dagger} | \Psi_{n}^{N-1} \rangle \langle \Psi_{n}^{N-1} | a_{p} | \Psi_{0}^{N} \rangle}{\omega + E_{n}^{N-1} - E_{0}^{N}}$$

$$\equiv G_{pq}^{+}(\omega) + G_{pq}^{-}(\omega)$$
(3)

where $G_{pq}^+(\omega)$ and $G_{pq}^-(\omega)$ are the forward and backward components of 1-GF describing electron attachment and detachment processes, respectively, $|\Psi_n^{N+1}\rangle$ and $|\Psi_n^{N-1}\rangle$ are the exact eigenstates of (N+1)- and (N-1)-electron systems with energies E_n^{N+1} and E_n^{N-1} .

Equation 3 shows that 1-GF contains information about the vertical electron attachment $(E_n^{N+1}-E_0^N)$ and ionization $(E_0^N-E_n^{N-1})$ energies, as well as the corresponding transition probabilities $(|\langle \Psi_0^N|a_p|\Psi_n^{N+1}\rangle|^2)$ and $|\langle \Psi_0^N|a_q^\dagger|\Psi_n^{N-1}\rangle|^2)$. For each component of 1-GF, the Lehmann representation can be compactly written in a matrix form as

$$\mathbf{G}_{\pm}(\omega) = \tilde{\mathbf{X}}_{\pm}(\omega \mathbf{1} - \tilde{\mathbf{\Omega}}_{\pm})^{-1} \tilde{\mathbf{X}}_{\pm}^{\dagger} \tag{4}$$

where $\tilde{\Omega}_{\pm}$ values are the diagonal matrices of exact vertical attachment $(\tilde{\Omega}_{+n}=E_n^{N+1}-E_0^N)$ and ionization $(\tilde{\Omega}_{-n}=E_0^N-E_n^{N-1})$ energies, while $\tilde{\mathbf{X}}_{\pm}$ are the matrices of

spectroscopic amplitudes with elements $\tilde{X}_{+pn} = \langle \Psi^N_0 | a_p | \Psi^{N+1}_n \rangle$ and $\tilde{X}_{-qn} = \langle \Psi^N_0 | a_q^\dagger | \Psi^{N-1}_n \rangle$.

2.2. General Overview of ADC for Charged Excitations. Although informative, eq 3 is not very useful for simulating charged excited states, since it assumes that the eigenstates $|\Psi_n^{N+1}\rangle$ and $|\Psi_n^{N-1}\rangle$ and their energies E_n^{N+1} and E_n^{N-1} are already known exactly! Calculating approximate charged excitation energies and transition probabilities by making approximations to 1-GF is the domain of propagator theory. Algebraic diagrammatic construction (ADC) is a particular propagator approach that obtains closed-form algebraic expressions for the 1-GF (or, in general, any propagator) approximated using low-order perturbation theory. $^{81,89-108}$

Two ADC variants for simulating charged excitations have been proposed. In the first one called the Dyson ADC framework, 81,89,116 the exact 1-GF in eq 3 is expressed in terms of the Green's function of a noninteracting system ($\mathbf{G}^{(0)}(\omega)$) via the Dyson equation $^{112-114}$

$$\mathbf{G}(\omega) = \mathbf{G}^{(0)}(\omega) + \mathbf{G}^{(0)}(\omega)\mathbf{\Sigma}(\omega)\mathbf{G}(\omega)$$

$$= \mathbf{G}^{(0)}(\omega) + \mathbf{G}^{(0)}(\omega)\mathbf{\Sigma}(\omega)\mathbf{G}^{(0)}(\omega)$$

$$+ \mathbf{G}^{(0)}(\omega)\mathbf{\Sigma}(\omega)\mathbf{G}^{(0)}(\omega)\mathbf{\Sigma}(\omega)\mathbf{G}^{(0)}(\omega) + \dots$$
(5)

where $\Sigma(\omega)$ is a frequency-dependent potential called self-energy, which contains information about all electron correlation effects in $G(\omega)$ that are not included in $G^{(0)}(\omega)$. In Dyson ADC, $\Sigma(\omega)$ is expressed as a sum of static (ω -independent, $\Sigma_s(\infty)$) and dynamic (ω -dependent, $\Sigma_d(\omega)$) contributions:

$$\Sigma(\omega) = \Sigma_{s}(\infty) + \Sigma_{d}(\omega) \tag{6}$$

The dynamic self-energy $\Sigma_{\rm d}(\omega)$ is expanded in a perturbative series, which is truncated at a low order n:

$$\Sigma_{\mathbf{d}}(\omega) \approx \Sigma_{\mathbf{d}}^{(0)}(\omega) + \Sigma_{\mathbf{d}}^{(1)}(\omega) + \dots + \Sigma_{\mathbf{d}}^{(n)}(\omega) \tag{7}$$

Taking advantage of the noninteracting nature of $G^{(0)}(\omega)$ (i.e., $G^{(0)}(\omega)$ corresponding to a Slater determinant wave function), Dyson ADC provides algebraic expressions for calculating the contributions to $\Sigma_{d}(\omega)$ at each order in perturbation theory. The resulting approximate $\Sigma_{\mathbf{d}}(\omega)$ is used to obtain the static self-energy $\Sigma_s(\infty)$ in eq 6, solve the Dyson eq 5 for approximate $G(\omega)$, and compute the corresponding charged excitation energies and transition probabilities. Since $G(\omega)$ in eq 5 is a sum of forward and backward components ($G(\omega)$ = $G_{+}(\omega) + G_{-}(\omega)$), in Dyson ADC, the electron-attached and ionized states are calculated simultaneously in a coupled basis of (N + 1)- and (N - 1)-electron configurations. In this respect, Dyson ADC is different from wave function-based theories (such as EOM-CC or Δ methods), which simulate the electron-attached and ionized states independently from each other.

In the second approach, termed non-Dyson ADC, 90-93,95-101,105-108 the energies and properties of charged electronic states are computed by directly approximating the spectral form of forward and backward 1-GF in eq 4, which can be written in a non-diagonal matrix representation

$$\mathbf{G}_{\pm}(\omega) = \mathbf{T}_{\pm}(\omega \mathbf{S}_{\pm} - \mathbf{M}_{\pm})^{-1} \mathbf{T}_{\pm}^{\dagger}$$
(8)

Similar to $\tilde{\mathbf{M}}_{\pm}$ and $\tilde{\mathbf{X}}_{\pm}$ in eq 4, the matrices \mathbf{M}_{\pm} and \mathbf{T}_{\pm} in eq 8 contain information about vertical charged excitation energies and transition probabilities, respectively, but are expressed in a different (noneigenstate) basis of (N+1)- and (N-1)-electron configurations $(|\Psi_{+\mu}\rangle)$ and $|\Psi_{-\mu}\rangle$. In the ADC literature, \mathbf{M}_{\pm} and \mathbf{T}_{\pm} are usually called the effective Hamiltonian and effective transition moments matrices, respectively. The \mathbf{S}_{\pm} matrices in eq 8 describe the overlap of (N+1)- and (N-1)-electron basis states within each set $(S_{\pm\mu\nu} = \langle \Psi_{\pm\mu}|\Psi_{\pm\nu}\rangle)$. Choosing $|\Psi_{+\mu}\rangle$ and $|\Psi_{-\mu}\rangle$ such that $\mathbf{G}_{+}(\omega)$ and $\mathbf{G}_{-}(\omega)$ do not couple, the \mathbf{M}_{\pm} , \mathbf{T}_{\pm} , and \mathbf{S}_{\pm} matrices are evaluated up to the order n in perturbation theory

$$\mathbf{M}_{+} \approx \mathbf{M}_{+}^{(0)} + \mathbf{M}_{+}^{(1)} + \dots + \mathbf{M}_{+}^{(n)}$$
 (9)

$$\mathbf{T}_{\pm} \approx \mathbf{T}_{\pm}^{(0)} + \mathbf{T}_{\pm}^{(1)} + \dots + \mathbf{T}_{\pm}^{(n)}$$
 (10)

$$S_{\pm} \approx S_{\pm}^{(0)} + S_{\pm}^{(1)} + \dots + S_{\pm}^{(n)}$$
 (11)

corresponding to the *n*th-order non-Dyson ADC approximation (ADC(*n*)). The ADC(*n*) charged excitation energies are computed as eigenvalues of the effective Hamiltonian matrices (Ω_+)

$$\mathbf{M}_{\pm}\mathbf{Y}_{\pm} = \mathbf{S}_{\pm}\mathbf{Y}_{\pm}\mathbf{\Omega}_{\pm} \tag{12}$$

Combining the eigenvectors \mathbf{Y}_{\pm} with the effective transition moments matrices \mathbf{T}_{\pm} allows one to obtain the ADC(n) spectroscopic amplitudes \mathbf{X}_{\pm}

$$\mathbf{X}_{\pm} = \mathbf{T}_{\pm} \mathbf{S}_{\pm}^{-1/2} \mathbf{Y}_{\pm} \tag{13}$$

and transition probabilities (also known as spectroscopic factors)

$$P_{\pm\mu} = \sum_{p} |X_{\pm p\mu}|^2 \tag{14}$$

which can be used to compute density of states

$$A(\omega) = -\frac{1}{\pi} \text{Im}[\text{Tr}\mathbf{G}_{\underline{+}}(\omega)]$$
(15)

and simulate photoelectron spectra. In addition, Y_{\pm} and X_{\pm} can be used to compute other useful properties of charged excited states (Section 3.5), such as electronic density difference, excited-state dipole moments, spin, and Dyson orbitals

$$|\phi_{\pm\mu}^{\rm Dyson}\rangle = \sum_{p} X_{\pm p\mu} |\phi_{p}\rangle \tag{16}$$

that are defined in the basis of reference molecular orbitals (ϕ_p) and are useful for interpreting transitions in photoelectron spectra.

While the Dyson and non-Dyson ADC approaches have been shown to produce similar numerical results at the same level of approximation (n), 93 the non-Dyson ADC framework allows for more computationally efficient and straightforward simulations of charged excitations by decoupling the forward and backward components of 1-GF and calculating the energies and properties of electron-attached and ionized states independently. Importantly, the non-Dyson ADC perturbation expansion in eqs 9 to 11 is generated by separating the total Hamiltonian (H) into zeroth-order $(H^{(0)})$ and perturbation contributions (V), $H = H^{(0)} + V$, and various choices of $H^{(0)}$ (and the corresponding zeroth-order reference wave function) are possible for a variety of applications. In the following, we

briefly review three formulations of non-Dyson ADC theory, namely: single-reference ADC for weakly correlated molecular systems (SR-ADC, Section 2.3), multireference ADC for molecules with multiconfigurational electronic structure (MR-ADC, Section 2.4), and periodic SR-ADC for crystalline materials (Section 2.5).

2.3. Single-Reference ADC. The single-reference formulation of non-Dyson ADC (SR-ADC) $^{90-93,95-101}$ starts by assuming that the ground-state electronic structure of a chemical system can be well described by a Slater determinant wave function obtained from a converged Hartree–Fock calculation ($|\Psi_0^N\rangle \approx |\Psi_{HF}\rangle$). As depicted in Figure 1a, the Slater

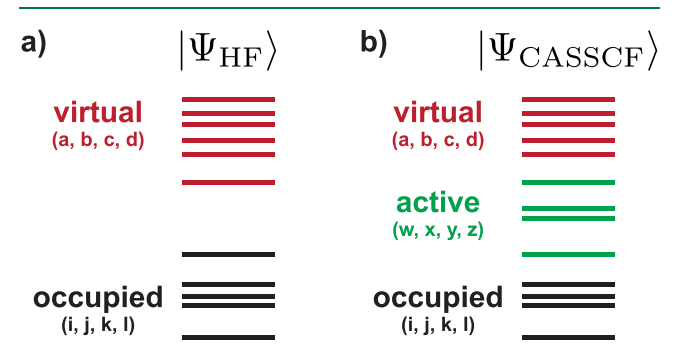


Figure 1. Schematic diagram representing molecular orbital spaces and their labeling for (a) the Hartree–Fock reference wave function in SR-ADC and (b) the CASSCF reference wave function in MR-ADC.

determinant $|\Psi_{\rm HF}\rangle$ is represented in a basis of occupied molecular orbitals (labeled as i, j, k, l, ...), with the remaining virtual orbitals left completely unoccupied (indexed as a, b, c, d, ...). Choosing the Fock operator as the zeroth-order Hamiltonian $H^{(0)}$ and incorporating all electron correlation effects in the perturbation operator V defines the order expansions for the ADC matrices in eqs 9 to 11 and the hierarchy of SR-ADC(n) approximations.

Working equations for the matrix elements of \mathbf{M}_{\pm} , \mathbf{T}_{\pm} , and \mathbf{S}_{\pm} are derived using one of two alternative theoretical frameworks, namely: (i) the intermediate state representation (ISR) $^{82-84}$ or (ii) the effective Liouvillian theory (EL). 86,96,109,110 These techniques offer different approaches for incorporating electron correlation effects and treating the coupling between $\mathbf{G}_{+}(\omega)$ and $\mathbf{G}_{-}(\omega)$ but result in numerically equivalent approximations at the same order in perturbation theory. We refer the readers to relevant publications for the details behind each approach. $^{82-84,86,96,109,110}$ In addition to deriving equations for \mathbf{M}_{\pm} , \mathbf{T}_{\pm} , and \mathbf{S}_{\pm} , both ISR and EL enable one to calculate density matrices and operator expectation

values, ^{98–100,104} which can be used to simulate excited-state properties (Section 3.5).

Figure 2 shows the structures of \mathbf{M}_{\pm} and \mathbf{T}_{\pm} for the low-order SR-ADC(n) approximations ($n \leq 3$). Regardless of the approach used to derive working equations, each matrix element can be assigned to one or a pair of excited electronic configurations denoted as $|\Psi_{\pm\mu}^{(k)}\rangle$, where k indicates a perturbation order. These ($N \pm 1$)-electron configurations are schematically depicted in Figure 3. The matrices of SR-

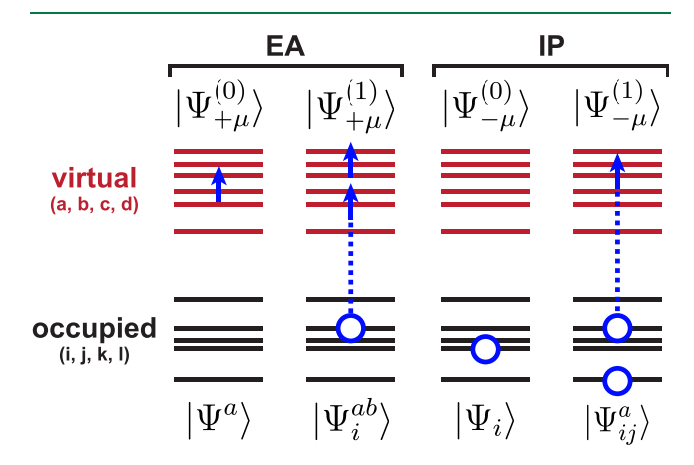


Figure 3. Schematic representation of the electron-attached $(|\Psi_{+\mu}^{(k)}\rangle)$ and ionized $(|\Psi_{-\mu}^{(k)}\rangle)$ electronic configurations used to represent charged excited states in low-order SR-ADC approximations. An arrow denotes electron attachment, a circle indicates ionization, while a circle connected with an arrow represents a single excitation.

ADC(0) and SR-ADC(1) approximations are expressed in the basis of zeroth-order states $|\Psi_{+\mu}^{(0)}\rangle$ and $|\Psi_{-\mu}^{(0)}\rangle$ that describe electron attachment to a virtual orbital and ionization of an occupied orbital, respectively (so-called 1p and 1h excitations). The first-order states $|\Psi_{\pm\mu}^{(1)}\rangle$ appearing in the equations of higher-order approximations (SR-ADC(n), $n \geq 2$) describe two-electron processes where attachment or ionization is accompanied by a one-electron excitation (2p-1h or 2h-1p). In SR-ADC, all basis states $|\Psi_{\pm\mu}^{(0)}\rangle$ are orthogonal to each other with $\mathbf{S}_{\pm}=\mathbf{1}$ at any level of approximation.

Each sector of \mathbf{M}_{\pm} corresponding to a pair of configurations $\langle \Psi_{\pm\mu}^{(k)}|$ and $|\Psi_{\pm\nu}^{(l)}\rangle$ (Figure 2) is evaluated up to the order m=n-k-l, where n is the level of SR-ADC(n) approximation. For example, the 1h/1h and 1p/1p blocks calculated with respect to $\langle \Psi_{\pm\mu}^{(0)}|$ and $|\Psi_{\pm\nu}^{(0)}\rangle$ are expanded up to the second order in SR-

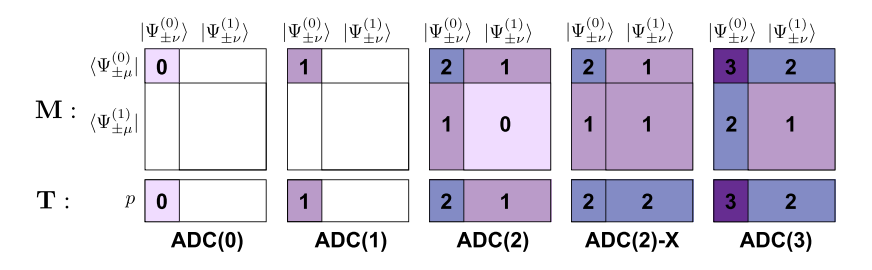


Figure 2. Perturbative structures of the effective Hamiltonian (M) and transition moments (T) matrices in the low-order ADC approximations. Numbers denote the perturbation order to which the effective Hamiltonian and transition moments are expanded for each sector. Shaded areas indicate nonzero blocks.

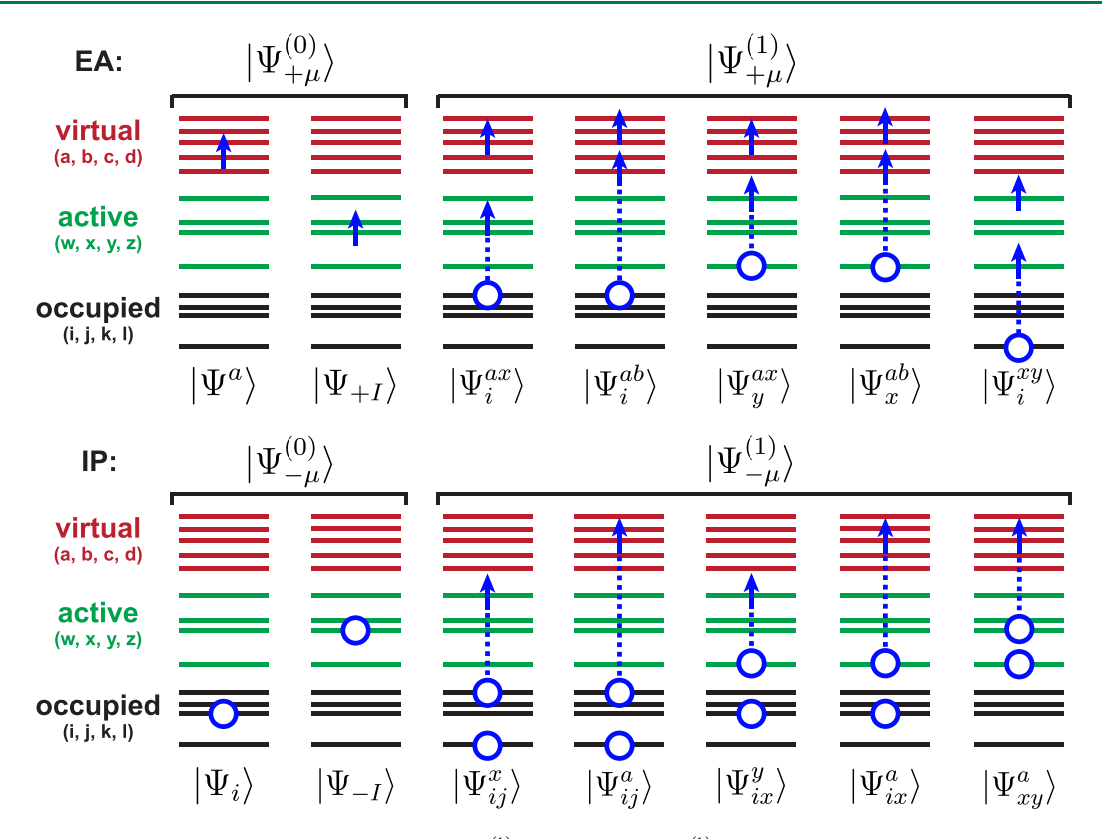


Figure 4. Schematic representation of the electron-attached $(|\Psi_{+\mu}^{(k)}\rangle)$ and ionized $(|\Psi_{-\mu}^{(k)}\rangle)$ electronic configurations used to represent charged excited states in low-order MR-ADC approximations. An arrow denotes electron attachment, a circle indicates ionization, while a circle connected with an arrow represents a single excitation.

ADC(2) and up to the third order in SR-ADC(3), while the 1h/2h-1p and 1p/2p-1h sectors are approximated to order one in SR-ADC(2) and order two in SR-ADC(3). The m=n-k-l restriction on the perturbation order is violated in the extended SR-ADC(2) approximation (SR-ADC(2)-X) where the 2p-1h/2p-1h and 2h-1p/2h-1p blocks are evaluated up to the first order in perturbation theory. This approach improves the description of orbital relaxation effects in the simulated excited electronic states but tends to exhibit larger errors in charged excitation energies compared to SR-ADC(2) due to a lack of error cancellation (Section 3.1). Similar to \mathbf{M}_{\pm} , the sectors of \mathbf{T}_{\pm} corresponding to different excited configurations $|\Psi_{\pm\mu}^{(k)}\rangle$ are expanded to order m=n-k.

The low-order SR-ADC(n) ($n \le 3$) methods for electron attachment and ionization have been implemented in the Q-Chem and PySCF software packages. At each order n, SR-ADC(n) is similar to nth-order Møller–Plesset perturbation theory (MPn) in computational cost. For a system with N_{occ} occupied and N_{vir} virtual molecular orbitals, the cost of SR-ADC(2) and SR-ADC(3) calculations scales as $O(N_{occ}^2 N_{vir}^3)$ and $O(N_{occ}^2 N_{vir}^4)$, respectively. The SR-ADC(2)-X method has the same computational scaling as SR-ADC(2) for charged excitation energies $(O(N_{occ}^2 N_{vir}^3))$ but is more expensive for calculating spectroscopic factors $(O(N_{occ}^2 N_{vir}^4))$. In practice, these additional costs can be avoided by neglecting expensive terms in T_{\pm} without significantly affecting the accuracy of SR-ADC(2)-X, resulting in the $O(N_{occ}^2 N_{vir}^3)$ computational scaling overall.

2.4. Multireference ADC. The performance of SR-ADC methods relies on the validity of Hartree–Fock approximation

and becomes unreliable when the ground-state electronic structure cannot be accurately represented with a single Slater determinant wave function. In addition, the low-order SR-ADC(n) approximations ($n \le 3$) show large errors in transition energies for doubly excited states and do not incorporate three-electron and higher excitations. This significantly reduces the accuracy of SR-ADC calculations for a wide range of important chemical systems, such as transition metal complexes, molecules with unpaired electrons, and highly conjugated organic compounds.

The multireference formulation of ADC (MR-ADC) $^{86,105-108,120}$ addresses these problems by describing the ground- and excited-state electronic structure with multiconfigurational wave functions. In MR-ADC, a subset of frontier molecular orbitals is selected to form an active space, as shown in Figure 1b. Next, the molecular orbitals are optimized in a complete active-space self-consistent field (CASSCF) $^{121-123}$ calculation that computes a multiconfigurational wave function for the reference (usually, ground) electronic state ($|\Psi^N_0\rangle\approx |\Psi_{CASSCF}\rangle$). To define the hierarchy of MR-ADC(n) approximations, the zeroth-order Hamiltonian $H^{(0)}$ is chosen to be the Dyall Hamiltonian, which incorporates all two-electron active-space interactions. Equations for the $\mathbf{M_{\pm}}$, $\mathbf{T_{\pm}}$, and $\mathbf{S_{\pm}}$ matrix elements ((9) to (11)) are derived using a multireference variant of the EL approach. 86

Incorporating multireference effects in the active space does not change the perturbative structure of ADC matrices (Figure 2) but introduces new classes of $(N \pm 1)$ -electron configurations $|\Psi_{\pm\mu}^{(0)}\rangle$ and $|\Psi_{\pm\mu}^{(1)}\rangle$ that do not appear in SR-ADC. ^{105,106} As shown in Figure 4, the MR-ADC zeroth-order

states $|\Psi_{\pm\mu}^{(0)}\rangle$ describe two kinds of charged excitations: (i) electron attachment or ionization in the active space and (ii) 1p or 1h excitations in the virtual or occupied orbitals, respectively. The active-space charged excitations are represented with complete active-space configuration interaction wave functions of the $(N \pm 1)$ -electron system $(|\Psi_{+}\rangle)$ computed using the reference CASSCF molecular orbitals. The 1p and 1h excited configurations ($|\Psi^a\rangle$ and $|\Psi_i\rangle$) are similar to the 1p and 1h excitations in SR-ADC (Figure 3) but are calculated with respect to the CASSCF wave function $|\Psi_{CASSCF}\rangle$ that incorporates multireference effects in the active space. Figure 4 shows that the first-order states $|\Psi_{+\mu}^{(1)}\rangle$ and $|\Psi_{-u}^{(1)}\rangle$ can be separated into five excitation classes that describe electron attachment or removal accompanied by a single excitation between occupied, active, or virtual orbitals. In contrast to SR-ADC, the excited configurations in Figure 4 are in general non-orthogonal, leading to non-diagonal overlap matrices S₊. 105,106

The ability to simulate excitations in all molecular orbitals distinguishes MR-ADC from other multireference perturbation theories (MRPT), such as CASPT2 or NEVPT2, 125-133 that cannot describe electronic transitions outside of active space. This makes MR-ADC particularly attractive for simulations of core-level excitations in X-ray spectroscopies (Section 3.2) 107,108 and chemical systems with high density of states. Additionally, unlike MRPT, MR-ADC offers a straightforward approach to calculate transition properties (e.g., spectroscopic factors, ionization cross sections, etc.) and can compute many excited states without averaging molecular orbitals in the CASSCF calculations.

The MR-ADC methods for charged excitations have been implemented up to the MR-ADC(2)-X level of theory (Figure 2). 105-108 In contrast to the accuracy of SR-ADC(2)-X relative to SR-ADC(2), the MR-ADC(2)-X method usually shows a better performance compared to MR-ADC(2) for electron attachment and ionization (Sections 3.1 and 3.2). For a fixed active space, the computational scaling of MR-ADC approximations is similar to that of SR-ADC and MRPT methods at each order in perturbation theory. Specifically, the computational cost of MR-ADC(2) and MR-ADC(2)-X charged excitation energies scales as $O(N_{occ+act}^2 N_{vir}^3)$, where $N_{occ+act}$ is the number of occupied and active orbitals, while N_{vir} is the size of virtual space. As in SR-ADC, simulating transition properties using MR-ADC(2)-X has a higher computational scaling, which can be lowered back to $O(N_{occ+act}^2 N_{vir}^3)$ by introducing minor approximations. The computational cost of MR-ADC(2) and MR-ADC(2)-X with respect to increasing the active space size (N_{act}) and the number of determinants in the complete active space (N_{det}) scales as $O(N_{det}N_{act}^{8})$, similar to CASPT2 or NEVPT2. As demonstrated in ref 106, this high computational scaling can be decreased to $O(N_{det}N_{act}^{6})$ by constructing efficient intermediates without introducing any approximations.

2.5. Periodic ADC. Although ADC originated in molecular quantum chemistry, it can be used to simulate the spectroscopic properties of periodic condensed matter systems, such as crystalline solids and low-dimensional materials. A periodic implementation of Dyson SR-ADC has been developed by Buth and co-workers who applied this approach to ionic crystals and one-dimensional molecular chains. ^{134–136}

Recently, we developed the non-Dyson SR-ADC for periodic systems and demonstrated its applications for a variety of materials from large-gap atomic and ionic solids to small-gap semiconductors.⁸⁷

In periodic non-Dyson SR-ADC, the Hamiltonian and 1-GF (eq 2) are expressed in a complex-valued basis set of crystalline molecular orbitals ^{137,138}

$$\left|\psi_{p\mathbf{k}}(\mathbf{r})\right\rangle = \sum_{\mu} c_{\mu p\mathbf{k}} \left|\phi_{\mu \mathbf{k}}(\mathbf{r})\right\rangle$$
 (17)

constructed as linear combinations of translation-symmetryadapted Gaussian atomic orbitals

$$\phi_{\mu \mathbf{k}}(\mathbf{r}) = \sum_{\mathbf{T}} e^{i\mathbf{k}\cdot\mathbf{T}} \chi_{\mu}(\mathbf{r} - \mathbf{T})$$
(18)

where $\chi_{\mu}(\mathbf{r}-\mathbf{T})$ are the atom-centered Gaussian basis functions, \mathbf{T} is a lattice translation vector, and \mathbf{k} is a crystal momentum vector in the first Brillouin zone. Similar to molecular ADC, the forward and backward contributions to 1-GF are written in a non-diagonal form

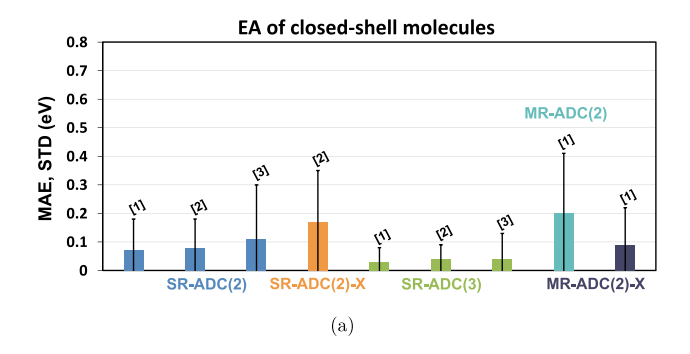
$$\mathbf{G}_{+}(\omega, \mathbf{k}) = \mathbf{T}_{+}(\mathbf{k})(\omega \mathbf{S}_{+}(\mathbf{k}) - \mathbf{M}_{+}(\mathbf{k}))^{-1} \mathbf{T}_{+}^{\dagger}(\mathbf{k})$$
(19)

where the ADC matrices acquire dependence on the crystal momentum **k**. Using the approach described in Section 2.3 and taking care of crystal momentum conservation allows one to derive the working equations of periodic SR-ADC(n) approximations for the matrix elements of $\mathbf{M}_{\pm}(\mathbf{k})$, $\mathbf{T}_{\pm}(\mathbf{k})$, and $\mathbf{S}_{\pm}(\mathbf{k})$. The crystal momentum dependence does not change the perturbative structure of ADC matrices (Figure 2) and the nature of electronic configurations that are used to represent charged excited states (Figure 3). As in molecular SR-ADC, in the periodic formulation, $\mathbf{S}_{\pm}(\mathbf{k}) = \mathbf{1}$ at any level of approximation.

The periodic non-Dyson SR-ADC(n) methods have been implemented in the PySCF package ¹¹⁸ up to the third order in perturbation theory ($n \leq 3$). ⁸⁷ Taking advantage of the crystalline translational symmetry, the SR-ADC(2) and SR-ADC(2)-X implementations have a $O(N_k^3 N_{occ}^2 N_{vir}^3)$ computational scaling, where N_{occ} and N_{vir} are the numbers of occupied and virtual orbitals per unit cell and N_k is the number of k-points sampled in the first Brillouin zone. The computational cost of periodic SR-ADC(3) is dominated by the noniterative calculation of ground-state wave function parameters, which scales as $O(N_k^4 N_{occ}^2 N_{vir}^4)$. For the remaining steps of the SR-ADC(3) algorithm, the computational scaling does not exceed $O(N_k^3 N_{occ}^2 N_{vir}^3)$.

3. CAPABILITIES AND ACCURACY OF ADC FOR CHARGED EXCITATIONS

3.1. Electron Affinities and Ionization Energies. The ADC calculations of charged excitations provide electron attachment and ionization energies that are computed by diagonalizing the effective Hamiltonian matrix in eq 12. Figures 5 and 6 show the error statistics for simulating vertical electron attachment and ionization energies of closed- and open-shell molecules using various levels of ADC theory, compiled from different benchmark studies. 93,96,97,99,100,102,104,106 For closed-shell systems, increasing the level of theory from SR-ADC(2) to SR-ADC(3) reduces the mean absolute error (MAE) in vertical charged excitation energies by a factor of 2 (Figures 5a and 6a). SR-ADC(3)



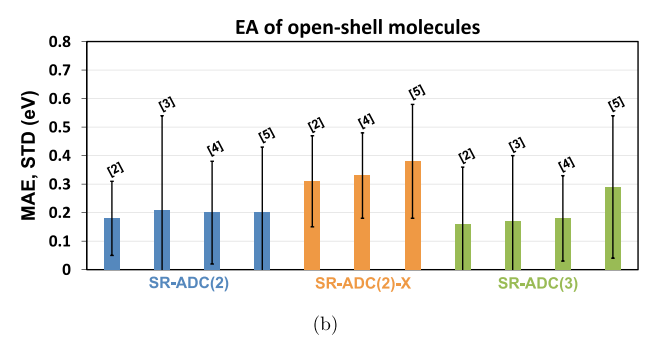
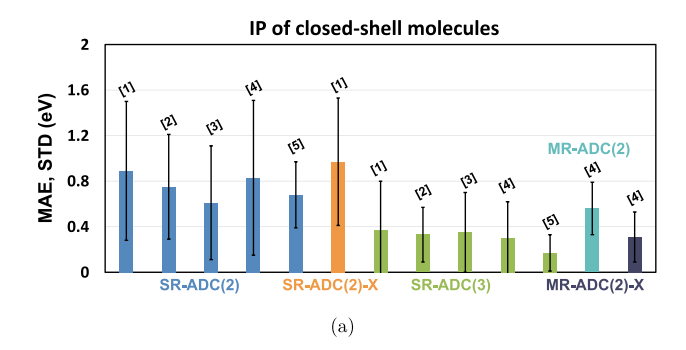


Figure 5. Mean absolute errors (MAEs, eV) and standard deviations (STDs, eV) in vertical electron attachment energies of (a) closed-shell and (b) open-shell molecules calculated using different levels of ADC theory. Open-shell calculations were performed using the unrestricted Hartree—Fock reference. MAEs are shown as colored boxes; black bars indicate STDs multiplied by a factor of 2. Data is compiled from different literature sources: [1] ref 106, [2] ref 96, [3] ref 100, [4] SR-ADC/UHF results for weakly spin-contaminated molecules from ref 104, and [5] SR-ADC/UHF results for strongly spin-contaminated molecules from ref 104.

shows the MAE of \sim 0.05 eV in electron affinities and \sim 0.35 eV in ionization energies. The performance of SR-ADC(2)-X is similar to SR-ADC(2) for ionization energies and is slightly worse than SR-ADC(2) for electron affinities.

Figures 5b and 6b demonstrate that the accuracy of SR-ADC calculations is different for molecules with unpaired electrons in the ground electronic state. These calculations, performed using the unrestricted Hartree–Fock (UHF) reference wave functions, present new challenges, such as an accurate description of electronic spin states and increased importance of electron correlation effects. Relative to closed-shell benchmark results, the average errors in vertical electron affinities of open-shell molecules increase 2-fold for SR-ADC(2) and SR-ADC(2)-X and by more than 3-fold for SR-ADC(3) (Figure 5b). Notably, the opposite trend is observed for the ionization energies of open-shell systems (Figure 6b) where the SR-ADC methods show a 2-fold decrease in MAE due to fortuitous error cancellation.

In a recent study, Stahl et al. investigated the effect of spin contamination in UHF reference wave function (ΔS^2) on the accuracy of open-shell SR-ADC calculations. Their results demonstrated that the charged excitation energies of SR-ADC(2) and SR-ADC(2)-X are relatively insensitive to spin contamination, while SR-ADC(3) is significantly less accurate for molecules with strongly spin-contaminated UHF references ($\Delta S^2 > 0.1$ au) where the errors in excitation energies increase by at least 60% (Figure 7). Combining SR-ADC(3) with restricted open-shell Hartree–Fock (ROHF) or orbital-



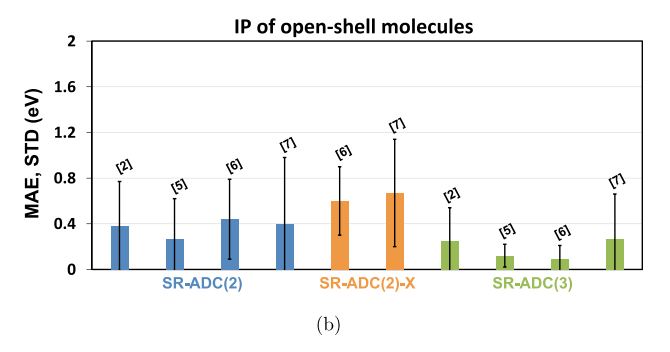
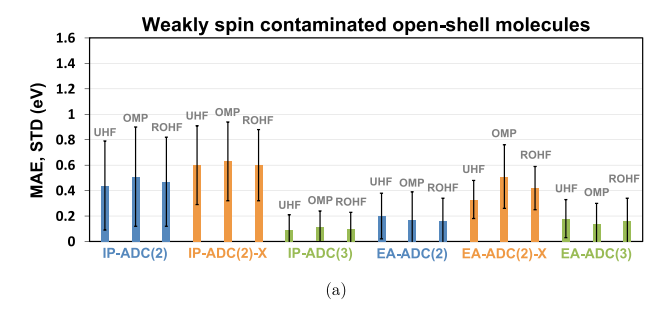


Figure 6. Mean absolute errors (MAEs, eV) and standard deviations (STDs, eV) in vertical ionization energies of (a) closed-shell and (b) open-shell molecules calculated using different levels of ADC theory. Open-shell calculations were performed using the unrestricted Hartree–Fock reference. MAEs are shown as colored boxes; black bars indicate STDs multiplied by a factor of 2. Data is compiled from different literature sources: [1] ref 93, [2] ref 99, [3] ref 102, [4] ref 106, [5] ref 97, [6] SR-ADC/UHF results for weakly spin-contaminated molecules from ref 104, and [7] SR-ADC/UHF results for strongly spin-contaminated molecules from ref 104.



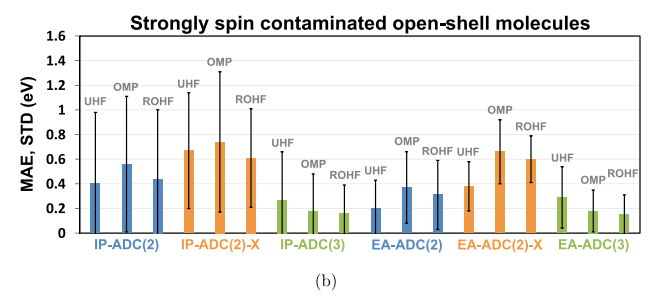


Figure 7. Mean absolute errors (MAEs, eV) and standard deviations (STDs, eV) in the SR-ADC vertical ionization and electron attachment energies for (a) 18 weakly and (b) 22 strongly spin-contaminated molecules with the ground-state UHF spin contamination of <0.1 and \geq 0.1 au, respectively. MAEs are shown as colored boxes; black bars indicate STDs multiplied by a factor of 2. Adapted from ref 104 with the permission of AIP Publishing. Copyright 2022.

optimized Møller–Plesset (OMP) reference wave functions improves performance for strongly spin-contaminated systems. As discussed in Section 3.5, this improvement correlates with a decrease in the ground- and excited-state spin contamination when using the ROHF or OMP reference orbitals.

The accuracy of MR-ADC methods for charged excitation energies has been benchmarked in refs 105 and 106 for a variety of small closed-shell molecules. Figures 5a and 6a show the MR-ADC benchmark data for equilibrium molecular geometries where the ground-state wave function is dominated by a single Slater determinant. In this case, MR-ADC(2)-X is consistently more accurate than MR-ADC(2) with MAE ranging between that of SR-ADC(2) and SR-ADC(3). Refs 105 and 106. also report benchmark results for molecules with multiconfigurational electronic structures. At stretched molecular geometries, the MAE of MR-ADC(2)-X in vertical ionization energies (0.25 eV) is more than ten times smaller than that of SR-ADC(3) (3.66 eV). For the C_2 molecule with a multireference ground state, SR-ADC(3) overestimates the first electron affinity by ~0.9 eV while MR-ADC(2)-X shows an error of ~0.25 eV, relative to accurate reference results from selected configuration interaction. 106

3.2. Core Ionization Energies. In addition to charged excitations in valence orbitals, ADC methods can be used to calculate the energies and properties of core-ionized states that are probed in X-ray photoelectron spectroscopy (XPS) experiments.²² These calculations require special numerical techniques to access core-level excited states that are deeply buried in the eigenstate spectrum of ADC effective Hamiltonian (eq 12). One such technique, termed corevalence separation (CVS) approximation, allows to compute high-energy core-excited states by neglecting their interaction with low-lying states originating from transitions in valence orbitals. The CVS approximation has been widely used in the ADC calculations of core ionization energies ^{89,91,92,151–158} with some studies exploring alternative variants of this technique. ^{96,107,108}

Several SR-ADC studies of core-ionized states have been reported. Angonoa et al. developed the first implementation of Dyson SR-ADC(4) and demonstrated its applications to K-shell (1s) ionization in N₂ and CO. Separate and co-workers presented non-Dyson SR-ADC(4) and showed that this method is equivalent to Dyson SR-ADC(4) within the CVS approximation. SR-ADC(4) method has been used to simulate core-ionized states in a variety of small molecules ranging from diatomics to DNA nucleobases. Separate In addition to CVS, a Green's function implementation of SR-ADC(3) has been used to compute the K-, L-, and M-shell ionization energies of a Zn atom.

Very recently, refs 107 and 108 reported a CVS implementation of MR-ADC(2) and MR-ADC(2)-X for simulating core ionization of molecules with multiconfigurational electronic structures. In contrast to conventional multireference theories, combining MR-ADC with CVS allows one to directly access core-ionized states without including core orbitals in the active space. Figure 8 shows the error statistics for core ionization energies of small molecules at equilibrium geometries calculated using selected SR- and MR-ADC methods, relative to accurate reference data from EOM-CCSDT. The best results are demonstrated by SR-ADC(2)-X and MR-ADC(2)-X methods, which show errors of less than 1 eV in core ionization energies. When using a small complete active space (CAS), the performance of MR-ADC methods is

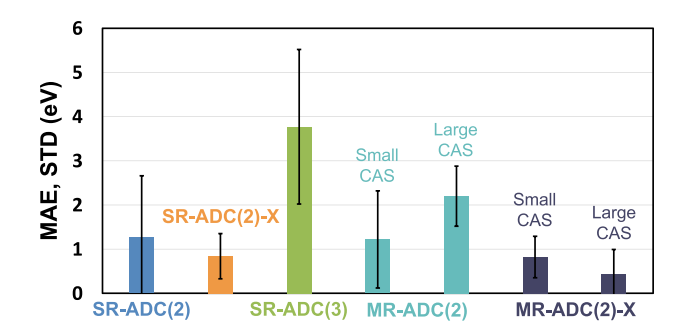


Figure 8. Mean absolute errors (MAEs, eV) and standard deviations (STDs, eV) in the K-edge core ionization energies of small molecules computed using the SR-ADC and MR-ADC methods, relative to reference EOM-CCSDT results. ¹⁴⁸ MAEs are shown as colored boxes,; black bars indicate STD multiplied by a factor of 2. Adapted from ref 108 with permission from the Royal Society of Chemistry. Copyright 2022.

very similar to that of SR-ADC. Increasing the size of CAS shifts the balance of error cancellation leading to larger MAE for MR-ADC(2) and smaller MAE for MR-ADC(2)-X.

The MR-ADC methods can be used to compute potential energy surfaces (PESs) of core-ionized states away from equilibrium geometries, which are useful for interpreting the results of time-resolved XPS experiments. Figure 9 demon-

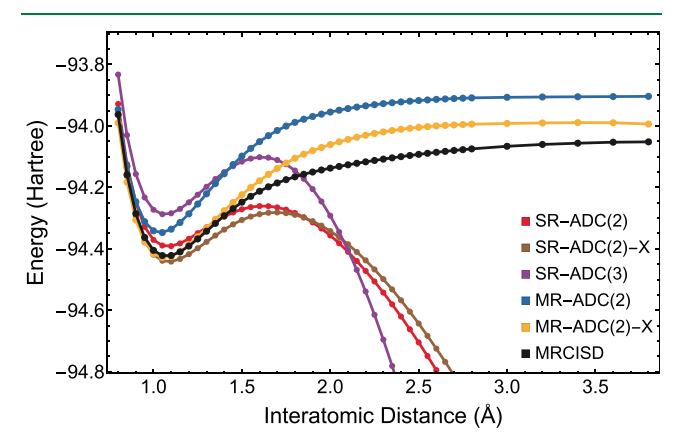


Figure 9. Potential energy curves for the K-edge core-ionized state of N_2 computed using the SR-ADC, MR-ADC, and MRCISD methods. Reproduced from ref 108 with permission from the Royal Society of Chemistry. Copyright 2022.

strates that MR-ADC(2) and MR-ADC(2)-X correctly predict the PES shape for the K-shell-ionized state of N_2 , in a good agreement with reference MRCISD calculations, while the core-ionized PESs computed using SR-ADC diverge away from the equilibrium region. 107,108

3.3. Photoelectron Spectra. The ADC methods allow one to efficiently simulate photoelectron spectra by calculating the density of states in eq 15. Several SR- and MR-ADC computations of molecular UV and X-ray photoelectron spectra have been reported. 97,98,101,105,107,108,151–157

Figure 10 compares the experimental photoelectron spectrum of the glycine molecule with the results of SR-ADC(3) calculations performed by Dempwolff and coworkers. ⁹⁷ Although the simulated spectrum does not incorporate vibrational effects, it reproduces the key features of the experimental spectrum quite well. Figure 11 shows the

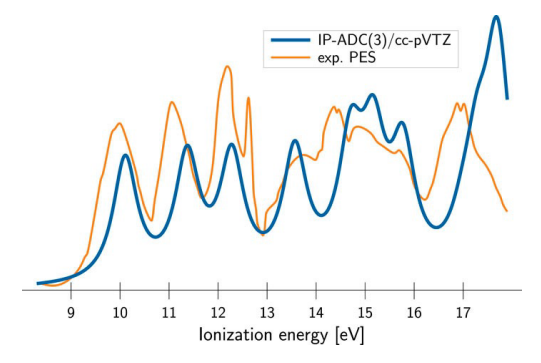


Figure 10. Photoelectron spectrum of the glycine molecule computed using SR-ADC(3) and compared to the experimental results. Seprinted from ref 97 with the permission of AIP Publishing. Copyright 2019.

results of SR-ADC(2) and SR-ADC(3) calculations for the open-shell TEMPO radical from ref 101. The computed spectra were shifted to reproduce the position of the first peak in the experimental data. Apart from this uniform shift, the SR-ADC(2) and SR-ADC(3) photoelectron spectra are in a good agreement with the experimental results. The SR-ADC(3) calculations show smaller errors in ionization energies and provide a better description of the photoelectron spectrum beyond 10 eV.

Examples of X-ray photoelectron spectra simulated using SR- and MR-ADC are shown in Figure 12 for the ozone molecule (O_3) . Although all ADC methods correctly predict the ordering and relative intensities of two peaks corresponding to the K-shell ionization of terminal and central oxygen atoms, the SR-ADC methods show large (>1 eV) errors in peak spacing relative to the experimental results. These errors originate from the multiconfigurational nature of the O_3 ground-state electronic structure, which presents challenges for single-reference theories such as SR-ADC. $^{162-169}$ The X-ray photoelectron spectra simulated using MR-ADC(2) and MR-ADC(2)-X are in a good agreement with experimental data showing less than 0.3 eV errors in peak spacing.

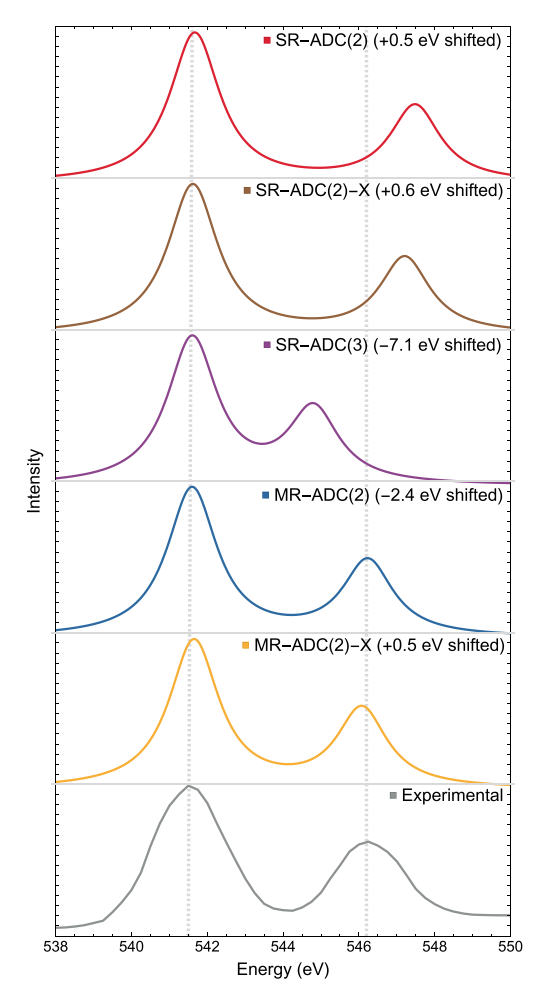
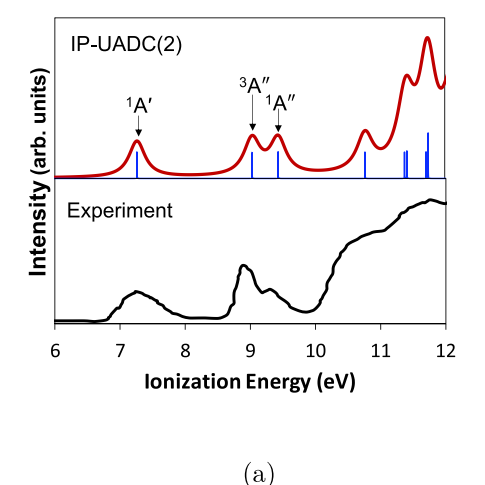


Figure 12. Oxygen K-edge X-ray photoelectron spectrum of ozone computed using the SR-ADC and MR-ADC methods compared to the experimental spectrum from ref 161. The simulated spectra used a 0.8 eV broadening parameter and were shifted to align with the first peak of the experimental spectrum. Reproduced from ref 108 with permission from the Royal Society of Chemistry. Copyright 2022.



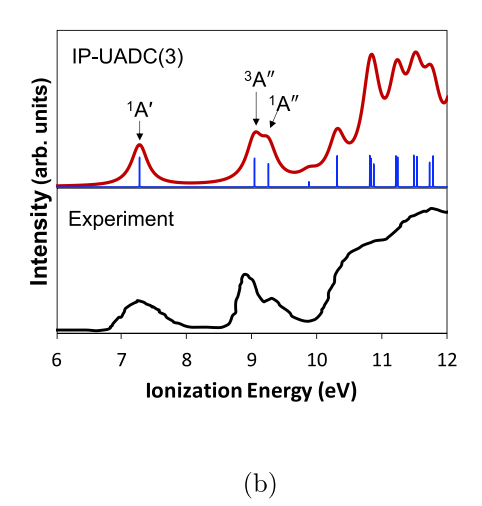


Figure 11. Photoelectron spectrum of the TEMPO radical computed using (a) SR-ADC(2) and (b) SR-ADC(3) and compared to the experimental results. The simulated spectra were shifted by (a) 1.02 and (b) -0.3 eV to reproduce the position of first peak in the experimental data. Reprinted from ref 101 with the permission of AIP Publishing. Copyright 2021.

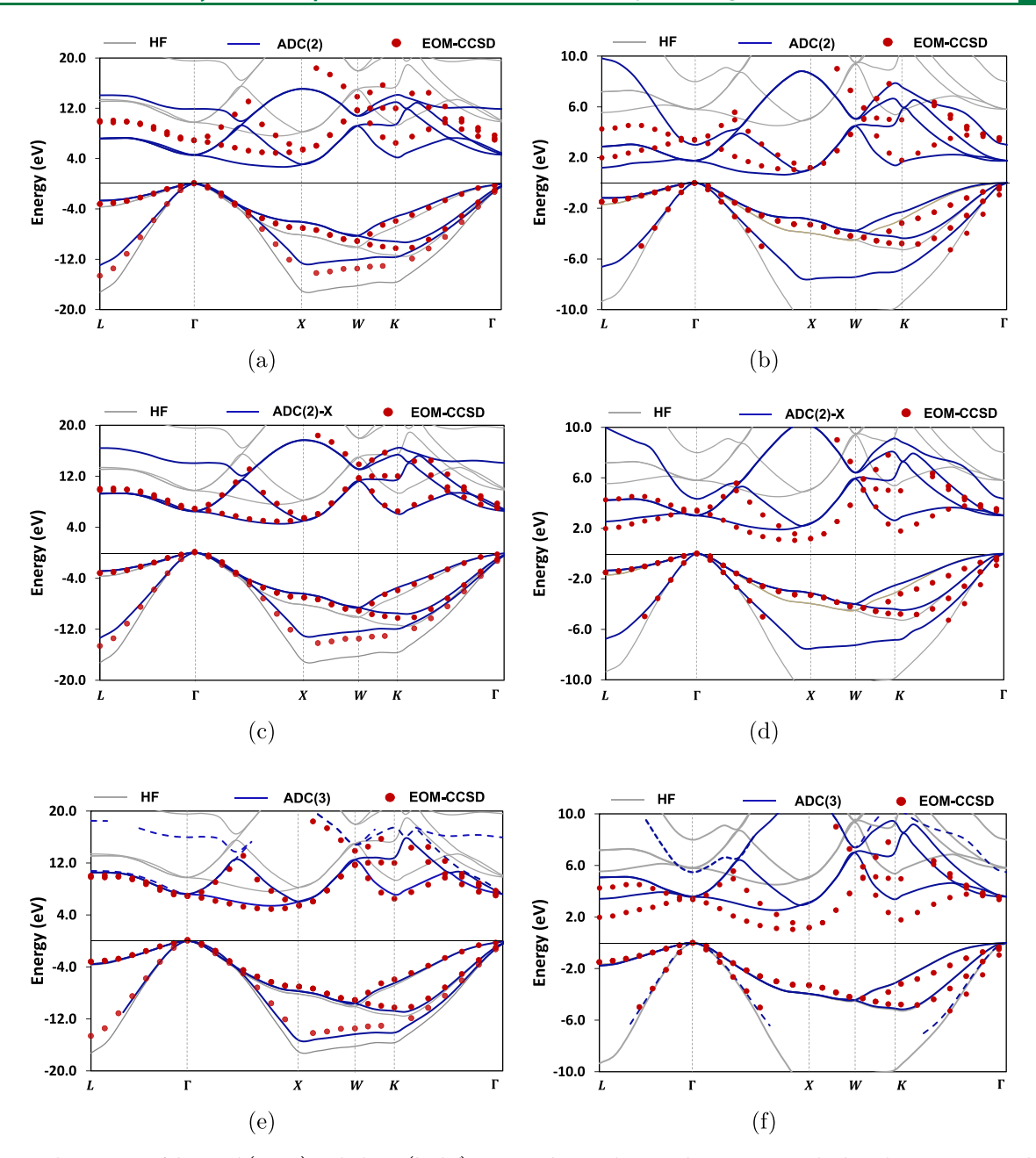


Figure 13. Band structures of diamond (a, c, e) and silicon (b, d, f) computed using the periodic SR-ADC methods with $3 \times 3 \times 3$ sampling of the Brillouin zone. Results are compared to the band structures calculated using the Hartree–Fock theory (HF) and equation-of-motion coupled cluster theory (EOM-CCSD). Adapted from ref 87. Copyright 2022 American Chemical Society.

3.4. Properties of Periodic Systems. When combined with periodic boundary conditions, the ADC methods can be used to elucidate the electronic structure of charged states in chemical systems with translational symmetry. Figure 13 shows the band structures of solid-state diamond and silicon computed using the periodic implementations of Hartree–Fock, SR-ADC, and EOM-CCSD methods with the $3 \times 3 \times 3$ k-point sampling of the first Brillouin zone. Each band structure plots the energies of charged electronic states as a function of crystal momentum k. For the diamond crystal with experimental band gap of ~ 5.5 eV, SR-ADC(2) correctly reproduces all features of the reference band structure from EOM-CCSD but underestimates the band gap by ~ 2.3 eV. The SR-ADC(2)-X and SR-ADC(3) methods improve the description of the band gap showing a very good agreement

with EOM-CCSD for all points in the band structure. The silicon crystal with experimental band gap of ~ 1.2 eV proves to be a more challenging test. In this case, the performance of all SR-ADC methods is nonuniform across different points of the first Brillouin zone, providing evidence that SR-ADC should be used with caution when applied to small-gap semiconductors like silicon.

These results are supported by benchmark data in Figure 14, which compares the SR-ADC band gaps extrapolated to the thermodynamic limit with the experimental results for seven semiconducting and insulating solids. The SR-ADC methods show good agreement with the experiment for large-gap materials such as Ne, LiF, and Ar. As the experimental band gap decreases, the performance of SR-ADC(2) deteriorates leading to large (~5 to 6 eV) errors for diamond, SiC, and

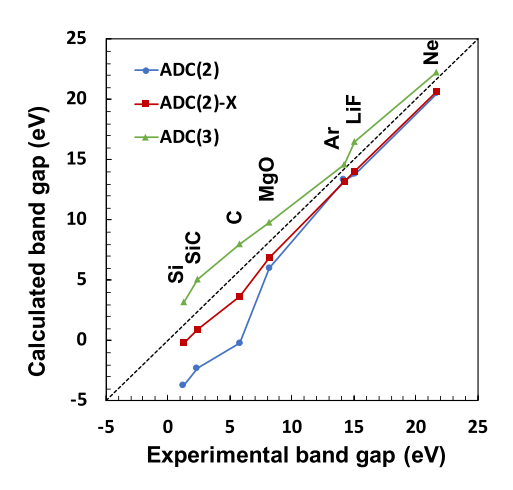


Figure 14. Fundamental band gaps computed using the periodic SR-ADC methods for seven semiconducting and insulating materials in comparison to experimental data. The experimental band gaps were corrected to exclude the effects of electron—phonon coupling. Reprinted from ref 87. Copyright 2022 American Chemical Society.

silicon. SR-ADC(2)-X and SR-ADC(3) significantly improve upon SR-ADC(2) showing errors that range from 1.5 to 2.7 eV relative to the experiment.

3.5. Other Properties of Charged Excited States. The ADC formalism allows one to compute a wide range of excited-state properties by providing access to wave functions and reduced density matrices of electronically excited states. Dempwolff and co-workers developed an approach based on intermediate state representation for calculating properties of electron-attached and detached states simulated using SR-ADC. P8-100 An alternative approach based on effective Liouvillian theory has been described by Stahl et al. To showcase the capabilities of ADC methods for calculating excited-state properties, we highlight the results from these recent studies below.

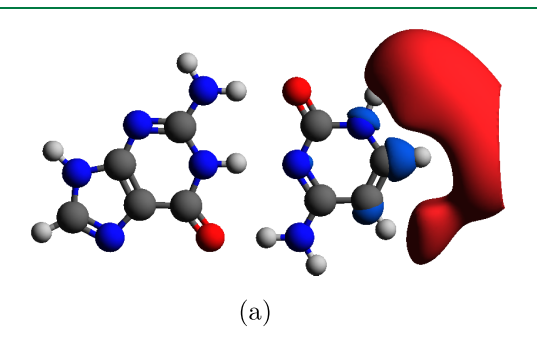
3.5.1. Dipole Moments. SR-ADC calculations of dipole moments for electron-attached and ionized states of molecules were reported by Dempwolff et al. $^{98-100}$ This work employed three SR-ADC approximations: SR-ADC(2), SR-ADC(3), and SR-ADC(3) with iterative fourth-order treatment of static self-energy (denoted as SR-ADC(3+)). All three SR-ADC methods predict accurate dipole moments of electron-attached states with mean absolute errors (MAEs) of \sim 12% to 16% relative to reference data from full configuration interaction. For the ionized states, the computed dipole moments show much stronger dependence on the level of theory. 98,99 In this case,

the SR-ADC(3+) method yields the most reliable results (MAE = 21%), while the average error increases 2-fold for SR-ADC(2) and SR-ADC(3). We note that in these studies the calculations of dipole moments were performed using the one-particle reduced density matrices evaluated up to the second order in single-reference perturbation theory. The importance of third-order correlation effects in the calculations of SR-ADC(3) and SR-ADC(3+) dipole moments remains to be studied.

3.5.2. Dyson Orbitals and Electronic Density Differences. The ADC methods enable direct calculations of Dyson orbitals (eq 16) that provide information about the spatial localization of an electron or hole created as a result of charged excitation and can be helpful in interpreting transitions in photoelectron spectra. Figure 15 shows Dyson orbitals for electron attachment to the guanine—cytosine DNA base pair computed at the neutral ground-state (a) and anion (b) equilibrium geometries using SR-ADC(3). At the neutral state geometry, the Dyson orbital reveals the dipole-bound nature of the electron-attached state with excess electron localized outside the molecule. Allowing the anion geometry to relax leads to a valence-bound state with electron localized on the π -orbitals of cytosine molecule.

As one-electron functions, Dyson orbitals are not able to describe charged excitations involving two or more electrons, such as low-intensity satellite transitions in photoelectron spectra, which are often difficult to interpret without the help from theoretical calculations. In this case, a more accurate picture of a charged excitation is provided by visualizing the change in electronic density between the ground and chargedexcited state, which can be calculated from the ADC excitedstate reduced density matrices and decomposed into detachment and attachment density contributions. 172 This is illustrated in Figure 16, which compares the SR-ADC(3) Dyson orbital with detachment and attachment densities for a satellite transition of galvinoxyl free radical (GFR).⁹⁸ Although the Dyson orbital suggests that this transition should be interpreted as removing an electron from the σ -orbitals of GFR, the density difference reveals a more complicated process with an $n \to \pi^*$ rearrangement of β -electron density and a $\pi \to$ σ^* excitation of α -electrons resulting in a positively charged hole with predominantly π -character.

3.5.3. Spin Properties. The ADC reduced density matrices can be used to compute excited-state expectation values for a variety of important observable properties. Recently, Stahl et al. investigated the accuracy of SR-ADC methods for simulating spin properties in charged states of open-shell molecules. They demonstrated that SR-ADC(2), SR-



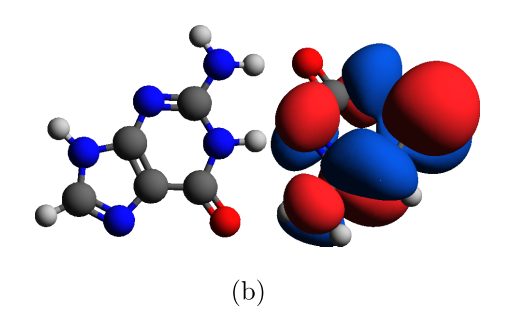


Figure 15. Dyson orbitals for the lowest-energy electron-attached state of the guanine—cytosine base pair at the neutral (a) and anion (b) equilibrium geometries computed using the SR-ADC(3) method. Reprinted from ref 101 with the permission of AIP Publishing. Copyright 2021.

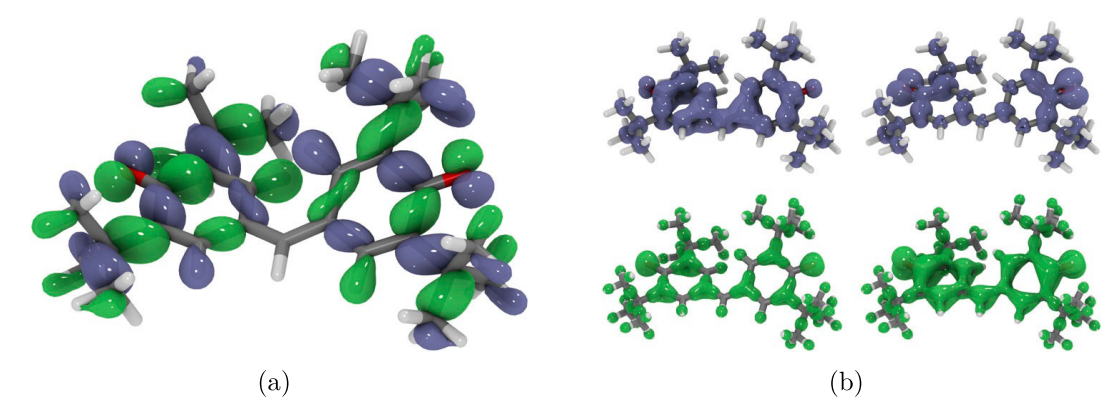
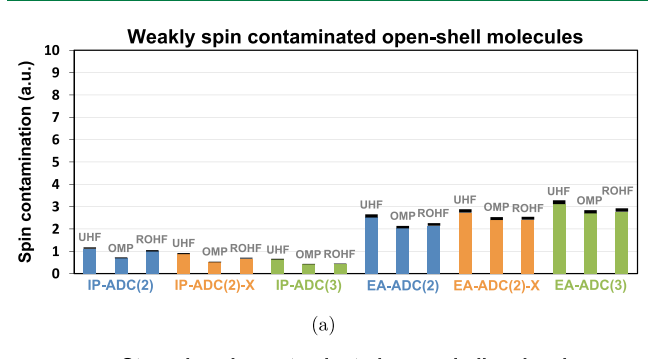


Figure 16. (a) Dyson orbital for a satellite transition in the photoelectron spectrum of galvinoxyl free radical (GFR) cation computed using SR-ADC(3). (b) The same transition is represented using detachment (upper row) and attachment (lower row) densities with the α (spin up) contributions shown on the left and the β (spin down) contributions shown on the right. Reprinted from ref 98 with the permission of AIP Publishing. Copyright 2020.

ADC(2)-X, and SR-ADC(3) exhibit non-negligible spin contamination in the calculated excited states. Figure 17



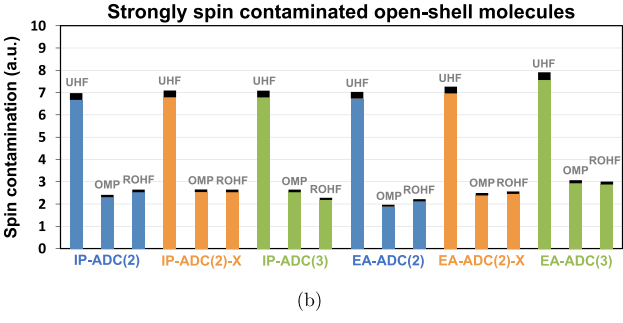


Figure 17. Spin contamination in the lowest-energy ionized and electron-attached states for (a) 18 weakly and (b) 22 strongly spin-contaminated molecules computed using SR-ADC with three different reference wave functions. Colored boxes indicate the sum of spin contamination for all molecules in each set; black boxes show the average spin contamination. Adapted from ref 104 with the permission of AIP Publishing. Copyright 2022.

shows that the excited-state spin contamination is relatively insensitive to the order of SR-ADC approximation and is particularly large for molecules with strong spin contamination in the UHF reference wave function ($\Delta S^2 > 0.1$ au). Performing SR-ADC calculations with the restricted openshell Hartree–Fock or orbital-optimized Møller–Plesset reference wave functions significantly reduces the excited-state spin contamination, although it does not cure it entirely. As shown in Figure 7, these improvements in describing spin properties lead to a noticeable increase in the SR-ADC(3) accuracy for charged excitation energies, while the performance

of SR-ADC(2) and SR-ADC(2)-X is affected to a much lesser extent (see Section 3.1 for more information). 104

4. SUMMARY AND OUTLOOK

In this Review, we discussed the current state of algebraic diagrammatic construction (ADC) theory for simulating charged excited states, focusing primarily on the non-Dyson formulation of this theoretical approach. ADC offers a compromise between accuracy of its approximations and computational cost, providing a hierarchy of systematically improvable and size-consistent methods for simulating many excited electronic states at the same time. The ADC methods allow one to compute spectroscopic observables (excitation energies and intensities in photoelectron spectra) and excitedstate properties (e.g., electronic density differences, dipole moments, spin) that can help assign features in experimental spectra, obtain deeper insight into excited-state electronic structure, and make reliable predictions of spectroscopic properties for future experiments. Recent developments of periodic and multireference variants of ADC have enabled applications of this theoretical approach to crystalline solids and chemical systems with complex, multiconfigurational electronic structures.

Looking ahead, the capabilities of ADC theory for simulating charged excited states can be expanded in many different directions. Applications to large molecular or crystalline systems require lowering the computational cost of ADC methods, which can be achieved by using local correlation, ^{173–175} frozen natural orbital, ^{176,177} or tensor factorization techniques. 178-180 Simulating charged excitations in realistic reaction environments necessitate the incorporation of environmental and solvation effects. 181 Characterizing potential energy surfaces of charged states would benefit from the implementation of analytical gradients. Additional developments are also needed for simulating core-ionized states and Xray photoelectron spectra where incorporating spin-orbit coupling effects can be important. Lastly, improved periodic ADC methods are necessary for accurate calculations of charged excitations in small-gap semiconductors where multireference effects play a significant role. Expanding these horizons will create new opportunities to advance our understanding of charged electronic states using ADC theory.

AUTHOR INFORMATION

Corresponding Author

Alexander Yu. Sokolov — Department of Chemistry and Biochemistry, The Ohio State University, Columbus, Ohio 43210, United States; orcid.org/0000-0003-2637-4134; Email: sokolov.8@osu.edu

Author

Samragni Banerjee — Department of Chemistry and Biochemistry, The Ohio State University, Columbus, Ohio 43210, United States

Complete contact information is available at: https://pubs.acs.org/10.1021/acs.jctc.3c00251

Notes

The authors declare no competing financial interest.

ACKNOWLEDGMENTS

An acknowledgment is made to the donors of the American Chemical Society Petroleum Research Fund for support (or partial support) of this research (PRF #65903-ND6). This work was also supported by the National Science Foundation, under Grant No. CHE-2044648. Additionally, S.B. was supported by a fellowship from Molecular Sciences Software Institute under NSF Grant No. ACI-1547580. Many calculations reported here were performed at the Ohio Supercomputer Center under projects PAS1583 and PAS1963. 182

REFERENCES

- (1) Ehring, H.; Karas, M.; Hillenkamp, F. Role of photoionization and photochemistry in ionization processes of organic molecules and relevance for matrix-assisted laser desorption lonization mass spectrometry. *Org. Mass Spectrom.* **1992**, *27*, 472–480.
- (2) Schermann, J.-P. Spectroscopy and modeling of biomolecular building blocks; Elsevier, 2007.
- (3) Wannier, G. H. The structure of electronic excitation levels in insulating crystals. *Phys. Rev.* **1937**, *52*, 191.
- (4) Illenberger, E. Electron-attachment reactions in molecular clusters. *Chem. Rev.* **1992**, *92*, 1589–1609.
- (5) Arnold, D.; Maroulis, A. Radical ions in photochemistry. 3. Photosensitized (electron transfer) cleavage of. beta.-phenethyl ethers. *J. Am. Chem. Soc.* **1976**, *98*, 5931–5937.
- (6) Bergmann, E. D. Ionization potentials of biological molecules. *Ann. N.Y. Acad. Sci.* **1969**, *158*, 140–147.
- (7) Scuseria, G. E. Advancing solid-state band gap predictions. *Proc. Natl. Acad. Sci. U.S.A.* **2021**, *118*, No. e2113648118.
- (8) Roca-Sanjuán, D.; Merchán, M.; Serrano-Andrés, L.; Rubio, M. Ab initio determination of the electron affinities of DNA and RNA nucleobases. *J. Chem. Phys.* **2008**, *129*, 095104.
- (9) Li, X.; Cai, Z.; Sevilla, M. D. DFT calculations of the electron affinities of nucleic acid bases: Dealing with negative electron affinities. *J. Phys. Chem. A* **2002**, *106*, 1596–1603.
- (10) Wesolowski, S. S.; Leininger, M. L.; Pentchev, P. N.; Schaefer, H. F. Electron affinities of the DNA and RNA bases. *J. Am. Chem. Soc.* **2001**, *123*, 4023–4028.
- (11) Richardson, N. A.; Wesolowski, S. S.; Schaefer, H. F. Electron affinity of the guanine- cytosine base pair and structural perturbations upon anion formation. *J. Am. Chem. Soc.* **2002**, *124*, 10163–10170.
- (12) Dutta, A. K.; Sengupta, T.; Vaval, N.; Pal, S. Electron attachment to DNA and RNA nucleobases: An EOMCC investigation. *Int. J. Quantum Chem.* **2015**, *115*, 753–764.
- (13) Aflatooni, K.; Gallup, G.; Burrow, P. Electron attachment energies of the DNA bases. *J. Phys. Chem. A* **1998**, *102*, 6205–6207.

- (14) Umstead, M. E.; Woods, F. J.; Johnson, J. E. A study of the ionization produced by the catalytic combustion of hydrocarbons. *J. Catal.* **1966**, *5*, 293–300.
- (15) Uddin, N.; Zhang, H.; Du, Y.; Jia, G.; Wang, S.; Yin, Z. Structural-phase catalytic redox reactions in energy and environmental applications. *Adv. Mater.* **2020**, *32*, 1905739.
- (16) Steenken, S. Purine bases, nucleosides, and nucleotides: aqueous solution redox chemistry and transformation reactions of their radical cations and e- and OH adducts. *Chem. Rev.* **1989**, *89*, 503–520.
- (17) Yan, M.; Becker, D.; Summerfield, S.; Renke, P.; Sevilla, M. D. Relative abundance and reactivity of primary ion radicals in. gamma-irradiated DNA at low temperatures. 2. Single-vs double-stranded DNA. *J. Phys. Chem.* **1992**, *96*, 1983–1989.
- (18) Colson, A.-O.; Sevilla, M. D. Structure and relative stability of deoxyribose radicals in a model DNA backbone: ab initio molecular orbital calculations. *J. Phys. Chem.* **1995**, *99*, 3867–3874.
- (19) Wintjens, R.; Liévin, J.; Rooman, M.; Buisine, E. Contribution of cation- π interactions to the stability of protein-DNA complexes. *J. Mol. Biol.* **2000**, 302, 393–408.
- (20) Huels, M. A.; Hahndorf, I.; Illenberger, E.; Sanche, L. Resonant dissociation of DNA bases by subionization electrons. *J. Chem. Phys.* **1998**, *108*, 1309–1312.
- (21) Hüfner, S. Photoelectron spectroscopy: principles and applications; Springer Science & Business Media, 2013.
- (22) Chastain, J.; King, Jr, R. C. Handbook of X-ray photoelectron spectroscopy; Perkin-Elmer Corporation, 1992; Vol. 40, p 221.
- (23) Bagus, P. S. Self-consistent-field wave functions for hole states of some Ne-like and Ar-like ions. *Phys. Rev.* **1965**, *139*, A619.
- (24) Deutsch, P.; Curtiss, L. Ab initio calculation of the K-shell excitation and ionization energies of CH₄, NH₃, H₂O, and HF. *Chem. Phys. Lett.* **1976**, *39*, 588–592.
- (25) Naves de Brito, A.; Correia, N.; Svensson, S.; Ågren, H. A theoretical study of x-ray photoelectron spectra of model molecules for polymethylmethacrylate. *J. Chem. Phys.* **1991**, 95, 2965–2974.
- (26) Schmitt, A.; Schirmer, J. Molecular K-shell excitation spectra in the relaxed-core Hartree-Fock approximation. *Chem. Phys.* **1992**, *164*, 1–9.
- (27) Besley, N. A.; Gilbert, A. T.; Gill, P. M. Self-consistent-field calculations of core excited states. *J. Chem. Phys.* **2009**, *130*, 124308.
- (28) Ambroise, M. A.; Jensen, F. Probing basis set requirements for calculating core ionization and core excitation spectroscopy by the Δ self-consistent-field approach. *J. Chem. Theory Comput.* **2019**, *15*, 325–337.
- (29) Ågren, H.; Jensen, H. J. A. Relaxation and correlation contributions to molecular double core ionization energies. *Chem. Phys.* **1993**, *172*, 45–57.
- (30) Triguero, L.; Plashkevych, O.; Pettersson, L.; Ågren, H. Separate state vs. transition state Kohn-Sham calculations of X-ray photoelectron binding energies and chemical shifts. *J. Electron Spectrosc. Relat. Phenom.* **1999**, *104*, 195–207.
- (31) Duflot, D.; Flament, J.-P.; Heinesch, J.; Hubin-Franskin, M.-J. The K-shell spectra of tetrahydrofuran studied by electron energy loss spectroscopy and abinitio calculations. *Chem. Phys. Lett.* **2010**, 495, 27–32.
- (32) Shim, J.; Klobukowski, M.; Barysz, M.; Leszczynski, J. Calibration and applications of the Δ MP2 method for calculating core electron binding energies. *Phys. Chem. Chem. Phys.* **2011**, *13*, 5703–5711.
- (33) Ljubić, I. Reliability of density functional and perturbation theories for calculating core-ionization spectra of free radicals. *J. Chem. Theory Comput.* **2014**, *10*, 2333–2343.
- (34) Su, N. Q.; Xu, X. Second-order perturbation theory for fractional occupation systems: Applications to ionization potential and electron affinity calculations. *J. Chem. Theory Comput.* **2016**, *12*, 2285–2297.
- (35) South, C.; Shee, A.; Mukherjee, D.; Wilson, A. K.; Saue, T. 4-Component relativistic calculations of L 3 ionization and excitations

- for the isoelectronic species UO_2^{2+} , OUN^+ and UN_2 . Phys. Chem. Chem. Phys. **2016**, 18, 21010–21023.
- (36) Śmiga, S.; Grabowski, I. Spin-component-scaled ΔMP2 parametrization: Toward a simple and reliable method for ionization energies. *J. Chem. Theory Comput.* **2018**, *14*, 4780–4790.
- (37) Holme, A.; Børve, K. J.; Sæthre, L. J.; Thomas, T. D. Accuracy of calculated chemical shifts in carbon 1s ionization energies from single-reference ab initio methods and density functional theory. *J. Chem. Theory Comput.* **2011**, *7*, 4104–4114.
- (38) Klues, M.; Hermann, K.; Witte, G. Analysis of the near-edge X-ray-absorption fine-structure of anthracene: A combined theoretical and experimental study. *J. Chem. Phys.* **2014**, *140*, 014302.
- (39) Zheng, X.; Cheng, L. Performance of Delta-Coupled-Cluster Methods for Calculations of Core-Ionization Energies of First-Row Elements. *J. Chem. Theory Comput.* **2019**, *15*, 4945–4955.
- (40) Jones, R. O.; Gunnarsson, O. The density functional formalism, its applications and prospects. *Rev. Mod. Phys.* **1989**, *61*, 689.
- (41) Roothaan, C. C. J. New Developments in Molecular Orbital Theory. *Rev. Mod. Phys.* **1951**, 23, 69–89.
- (42) Szabo, A.; Ostlund, N. S. Modern quantum chemistry: introduction to advanced electronic structure theory; Courier Corporation, 2012.
- (43) Helgaker, T.; Jorgensen, P.; Olsen, J. Molecular electronic-structure theory; John Wiley & Sons, 2013.
- (44) Runge, E.; Gross, E. K. U. Density-Functional Theory for Time-Dependent Systems. *Phys. Rev. Lett.* **1984**, *52*, 997–1000.
- (45) Besley, N. A.; Asmuruf, F. A. Time-dependent density functional theory calculations of the spectroscopy of core electrons. *Phys. Chem. Phys.* **2010**, *12*, 12024–12039.
- (46) Akama, T.; Nakai, H. Short-time Fourier transform analysis of real-time time-dependent Hartree—Fock and time-dependent density functional theory calculations with Gaussian basis functions. *J. Chem. Phys.* **2010**, *132*, 054104.
- (47) Lopata, K.; Van Kuiken, B. E.; Khalil, M.; Govind, N. Linear-response and real-time time-dependent density functional theory studies of core-level near-edge x-ray absorption. *J. Chem. Theory Comput.* **2012**, *8*, 3284–3292.
- (48) Herbert, J. M. In Theoretical and Computational Photochemistry: Fundamentals, Methods, Applications and Synergy with Experimental Approaches; García-Iriepa, C., Marazzi, M., Eds.; Elsevier, 2023; Chapter 3.
- (49) McKechnie, S.; Booth, G. H.; Cohen, A. J.; Cole, J. M. On the accuracy of density functional theory and wave function methods for calculating vertical ionization energies. *J. Chem. Phys.* **2015**, *142*, 194114.
- (50) Nguyen, H.-V.; Pham, T. A.; Rocca, D.; Galli, G. Improving accuracy and efficiency of calculations of photoemission spectra within the many-body perturbation theory. *Phys. Rev. B* **2012**, *85*, 081101.
- (51) Hedin, L. New method for calculating the one-particle Green's function with application to the electron-gas problem. *Phys. Rev. A* **1965**, *139*, A796–A823.
- (52) Faleev, S. V.; van Schilfgaarde, M.; Kotani, T. All-Electron Self-Consistent GW Approximation: Application to Si, MnO, and NiO. *Phys. Rev. Lett.* **2004**, *93*, 126406.
- (53) van Schilfgaarde, M.; Kotani, T.; Faleev, S. Quasiparticle Self-Consistent GW Theory. *Phys. Rev. Lett.* **2006**, *96*, 226402.
- (54) van Setten, M. J.; Weigend, F.; Evers, F. The GW-Method for Quantum Chemistry Applications: Theory and Implementation. *J. Chem. Theory Comput.* **2013**, *9*, 232–246.
- (55) Reining, L. The GW approximation: content, successes and limitations. WIREs Comput. Mol. Sci. 2018, 8, No. e1344.
- (56) Linderberg, J.; Öhrn, Y. Propagators in quantum chemistry; John Wiley & Sons, 2004.
- (57) Cederbaum, L.; Domcke, W. Theoretical aspects of ionization potentials and photoelectron spectroscopy: A Green's function approach. *Adv. Chem. Phys.* **2007**, *36*, 205–344.

- (58) Ortiz, J. V. Electron propagator theory: an approach to prediction and interpretation in quantum chemistry. *WIREs Comput. Mol. Sci.* **2013**, *3*, 123–142.
- (59) Nakatsuji, H.; Hirao, K. Cluster expansion of the wavefunction. Symmetry-adapted-cluster expansion, its variational determination, and extension of open-shell orbital theory. *J. Chem. Phys.* **1978**, *68*, 2053–2065.
- (60) Nakatsuji, H. Cluster expansion of the wavefunction. Electron correlations in ground and excited states by SAC (symmetry-adapted-cluster) and SAC CI theories. *Chem. Phys. Lett.* **1979**, *67*, 329–333.
- (61) Asmuruf, F. A.; Besley, N. A. Calculation of near-edge X-ray absorption fine structure with the CIS (D) method. *Chem. Phys. Lett.* **2008**, 463, 267–271.
- (62) Maganas, D.; DeBeer, S.; Neese, F. Restricted open-shell configuration interaction cluster calculations of the L-edge x-ray absorption study of TiO₂ and CaF₂ solids. *Inorg. Chem.* **2014**, *53*, 6374–6385.
- (63) Toffoli, D.; Decleva, P. A Multichannel Least-Squares B-Spline Approach to Molecular Photoionization: Theory, Implementation, and Applications within the Configuration—Interaction Singles Approximation. *J. Chem. Theory Comput.* **2016**, *12*, 4996—5008.
- (64) Ehlert, C.; Klamroth, T. The quest for best suited references for configuration interaction singles calculations of core excited states. *J. Comput. Chem.* **2017**, *38*, 116–126.
- (65) Kuramoto, K.; Ehara, M.; Nakatsuji, H. Theoretical fine spectroscopy with symmetry adapted cluster—configuration interaction general-R method: First-row K-shell ionizations and their satellites. *J. Chem. Phys.* **2005**, *122*, 014304.
- (66) Ehara, M.; Kuramoto, K.; Nakatsuji, H. Relativistic effects in K-shell ionizations: SAC-CI general-R study based on the DK2 Hamiltonian. *Chem. Phys.* **2009**, *356*, 195–198.
- (67) Sekino, H.; Bartlett, R. J. A linear response, coupled-cluster theory for excitation energy. *Int. J. Quantum Chem.* **1984**, *26*, 255–265.
- (68) Sauer, S. P.; Schreiber, M.; Silva-Junior, M. R.; Thiel, W. Benchmarks for electronically excited states: a comparison of noniterative and iterative triples corrections in linear response coupled cluster methods: CCSDR (3) versus CC3. J. Chem. Theory Comput. 2009, 5, 555–564.
- (69) Rocha-Rinza, T.; Christiansen, O. Linear response coupled cluster study of the benzene excimer. *Chem. Phys. Lett.* **2009**, 482, 44–49.
- (70) Koch, H.; Jensen, H. J. A.; Jorgensen, P.; Helgaker, T. Excitation energies from the coupled cluster singles and doubles linear response function (CCSDLR). Applications to Be, CH^+ , CO, and H_2O . *J. Chem. Phys.* **1990**, 93, 3345–3350.
- (71) Piecuch, P.; Kondo, A. E.; Spirko, V.; Paldus, J. Molecular quadrupole moment functions of HF and N₂. I. Ab initio linear-response coupled-cluster results. *J. Chem. Phys.* **1996**, *104*, 4699–4715.
- (72) Nooijen, M.; Snijders, J. G. Coupled cluster approach to the single-particle Green's function. *Int. J. Quantum Chem.* **1992**, 44, 55–83.
- (73) Nooijen, M.; Snijders, J. G. Coupled cluster Green's function method: Working equations and applications. *Int. J. Quantum Chem.* **1993**, *48*, 15–48.
- (74) Nooijen, M.; Snijders, J. G. Second order many-body perturbation approximations to the coupled cluster Green's function. *J. Chem. Phys.* **1995**, *102*, 1681–1688.
- (75) Stanton, J. F.; Bartlett, R. J. The equation of motion coupled-cluster method. A systematic biorthogonal approach to molecular excitation energies, transition probabilities, and excited state properties. J. Chem. Phys. 1993, 98, 7029.
- (76) Krylov, A. I. Equation-of-motion coupled-cluster methods for open-shell and electronically excited species: The hitchhiker's guide to Fock space. *Annu. Rev. Phys. Chem.* **2008**, *59*, 433–462.
- (77) Kowalski, K.; Bhaskaran-Nair, K.; Shelton, W. A. Coupledcluster representation of Green function employing modified spectral

- resolutions of similarity transformed Hamiltonians. J. Chem. Phys. 2014, 141, 094102.
- (78) Bhaskaran-Nair, K.; Kowalski, K.; Shelton, W. A. Coupled cluster Green function: Model involving single and double excitations. *J. Chem. Phys.* **2016**, *144*, 144101.
- (79) Peng, B.; Kowalski, K. Green's Function Coupled-Cluster Approach: Simulating Photoelectron Spectra for Realistic Molecular Systems. *J. Chem. Theory Comput.* **2018**, *14*, 4335–4352.
- (80) Schirmer, J. Beyond the random-phase approximation: A new approximation scheme for the polarization propagator. *Phys. Rev. A* **1982**, *26*, 2395–2416.
- (81) Schirmer, J.; Cederbaum, L. S.; Walter, O. New approach to the one-particle Green's function for finite Fermi systems. *Phys. Rev. A* 1983, 28, 1237–1259.
- (82) Schirmer, J. Closed-form intermediate representations of many-body propagators and resolvent matrices. *Phys. Rev. A* **1991**, 43, 4647–4659.
- (83) Mertins, F.; Schirmer, J. Algebraic propagator approaches and intermediate-state representations. I. The biorthogonal and unitary coupled-cluster methods. *Phys. Rev. A* **1996**, *53*, 2140–2152.
- (84) Schirmer, J.; Trofimov, A. B. Intermediate state representation approach to physical properties of electronically excited molecules. *J. Chem. Phys.* **2004**, *120*, 11449–11464.
- (85) Dreuw, A.; Wormit, M. The algebraic diagrammatic construction scheme for the polarization propagator for the calculation of excited states. WIREs Comput. Mol. Sci. 2015, 5, 82–95.
- (86) Sokolov, A. Y. Multi-reference algebraic diagrammatic construction theory for excited states: General formulation and first-order implementation. *J. Chem. Phys.* **2018**, *149*, 204113.
- (87) Banerjee, S.; Sokolov, A. Y. Non-Dyson Algebraic Diagrammatic Construction Theory for Charged Excitations in Solids. *J. Chem. Theory Comput.* **2022**, *18*, 5337–5348.
- (88) Møller, C.; Plesset, M. S. Note on an Approximation Treatment for Many-Electron Systems. *Phys. Rev.* **1934**, *46*, 618–622.
- (89) Angonoa, G.; Walter, O.; Schirmer, J. Theoretical K-shell ionization spectra of N2 and CO by a fourth-order Green's function method. *J. Chem. Phys.* **1987**, *87*, *6789*–*6801*.
- (90) Schirmer, J.; Trofimov, A. B.; Stelter, G. A non-Dyson third-order approximation scheme for the electron propagator. *J. Chem. Phys.* **1998**, *109*, 4734.
- (91) Schirmer, J.; Thiel, A. An intermediate state representation approach to K-shell ionization in molecules. I. Theory. *J. Chem. Phys.* **2001**, *115*, 10621–10635.
- (92) Thiel, A.; Schirmer, J.; Köppel, H. An intermediate state representation approach to K-shell ionization in molecules. II. Computational tests. *J. Chem. Phys.* **2003**, *119*, 2088–2101.
- (93) Trofimov, A. B.; Schirmer, J. Molecular ionization energies and ground- and ionic-state properties using a non-Dyson electron propagator approach. *J. Chem. Phys.* **2005**, *123*, 144115.
- (94) Knippenberg, S.; Rehn, D. R.; Wormit, M.; Starcke, J. H.; Rusakova, I. L.; Trofimov, A. B.; Dreuw, A. Calculations of nonlinear response properties using the intermediate state representation and the algebraic-diagrammatic construction polarization propagator approach: Two-photon absorption spectra. *J. Chem. Phys.* **2012**, 136, 064107.
- (95) Schneider, M.; Soshnikov, D. Y.; Holland, D. M. P.; Powis, I.; Antonsson, E.; Patanen, M.; Nicolas, C.; Miron, C.; Wormit, M.; Dreuw, A.; Trofimov, A. B. A fresh look at the photoelectron spectrum of bromobenzene: A third-order non-Dyson electron propagator study. *J. Chem. Phys.* **2015**, *143*, 144103.
- (96) Banerjee, S.; Sokolov, A. Y. Third-order algebraic diagrammatic construction theory for electron attachment and ionization energies: Conventional and Green's function implementation. *J. Chem. Phys.* **2019**, *151*, 224112.
- (97) Dempwolff, A. L.; Schneider, M.; Hodecker, M.; Dreuw, A. Efficient implementation of the non-Dyson third-order algebraic diagrammatic construction approximation for the electron propagator for closed- and open-shell molecules. *J. Chem. Phys.* **2019**, *150*, 064108.

- (98) Dempwolff, A. L.; Paul, A. C.; Belogolova, A. M.; Trofimov, A. B.; Dreuw, A. Intermediate state representation approach to physical properties of molecular electron-detached states. I. Theory and implementation. *J. Chem. Phys.* **2020**, *152*, 024113.
- (99) Dempwolff, A. L.; Paul, A. C.; Belogolova, A. M.; Trofimov, A. B.; Dreuw, A. Intermediate state representation approach to physical properties of molecular electron-detached states. II. Benchmarking. *J. Chem. Phys.* **2020**, *152*, 024125.
- (100) Dempwolff, A. L.; Belogolova, A. M.; Trofimov, A. B.; Dreuw, A. Intermediate state representation approach to physical properties of molecular electron-attached states: Theory, implementation, and benchmarking. *J. Chem. Phys.* **2021**, *154*, 104117.
- (101) Banerjee, S.; Sokolov, A. Y. Efficient implementation of the single-reference algebraic diagrammatic construction theory for charged excitations: Applications to the TEMPO radical and DNA base pairs. *J. Chem. Phys.* **2021**, *154*, 074105.
- (102) Dempwolff, A. L.; Hodecker, M.; Dreuw, A. Vertical ionization potential benchmark for unitary coupled-cluster and algebraic-diagrammatic construction methods. *J. Chem. Phys.* **2022**, *156*, 054114.
- (103) Liu, J.; Hättig, C.; Höfener, S. Analytical nuclear gradients for electron-attached and electron-detached states for the second-order algebraic diagrammatic construction scheme combined with frozendensity embedding. *J. Chem. Phys.* **2020**, *152*, 174109.
- (104) Stahl, T. L.; Banerjee, S.; Sokolov, A. Y. Quantifying and reducing spin contamination in algebraic diagrammatic construction theory of charged excitations. *J. Chem. Phys.* **2022**, *157*, 044106.
- (105) Chatterjee, K.; Sokolov, A. Y. Second-Order Multireference Algebraic Diagrammatic Construction Theory for Photoelectron Spectra of Strongly Correlated Systems. *J. Chem. Theory Comput.* **2019**, *15*, 5908–5924.
- (106) Chatterjee, K.; Sokolov, A. Y. Extended Second-Order Multireference Algebraic Diagrammatic Construction Theory for Charged Excitations. *J. Chem. Theory Comput.* **2020**, *16*, 6343–6357.
- (107) de Moura, C. E. V.; Sokolov, A. Y. Simulating X-ray photoelectron spectra with strong electron correlation using multi-reference algebraic diagrammatic construction theory. *Phys. Chem. Chem. Phys.* **2022**, 24, 4769–4784.
- (108) de Moura, C. E. V.; Sokolov, A. Y. Correction: Simulating X-ray photoelectron spectra with strong electron correlation using multireference algebraic diagrammatic construction theory. *Phys. Chem. Chem. Phys.* **2022**, *24*, 8041–8046.
- (109) Prasad, M. D.; Pal, S.; Mukherjee, D. Some aspects of self-consistent propagator theories. *Phys. Rev. A* **1985**, *31*, 1287.
- (110) Mukherjee, D.; Kutzelnigg, W. An Effective Liouvillean Formalism for Propagators in Fock Space: Connection with Effective Hamiltonian Approach for Energy Differences. In *Many-Body Methods in Quantum Chemistry*; Springer, 1989; Vol. 52, pp 257–274.
- (111) Meissner, L.; Bartlett, R. J. Electron propagator theory with the ground state correlated by the coupled-cluster method. *Int. J. Quantum Chem.* **1993**, 48, 67–80.
- (112) Fetter, A. L.; Walecka, J. D. Quantum theory of many-particle systems; Dover Publications, 1971.
- (113) Dickhoff, W. H.; Van Neck, D. V. Many-body theory exposed! Propagator description of quantum mechanics in many-body systems; World Scientific Publishing Company, 2008.
- (114) Schirmer, J. Many-body methods for atoms, molecules and clusters; Springer, 2018.
- (115) Kobe, D. H. Spectral representation of the many-time, causal Green's function in nonrelativistic many-body theory. *Ann. Phys.* **1962**, *19*, 448–457.
- (116) Santra, R.; Kryzhevoi, N. V.; Cederbaum, L. S. X-ray two-photon photoelectron spectroscopy: a theoretical study of inner-shell spectra of the organic para-aminophenol molecule. *Phys. Rev. Lett.* **2009**, *103*, 013002.
- (117) Epifanovsky, E.; Gilbert, A. T. B.; Feng, X.; Lee, J.; Mao, Y.; Mardirossian, N.; Pokhilko, P.; White, A. F.; Coons, M. P.; Dempwolff, A. L.; Gan, Z.; Hait, D.; Horn, P. R.; Jacobson, L. D.; Kaliman, I.; Kussmann, J.; Lange, A. W.; Lao, K. U.; Levine, D. S.; Liu,

J.; McKenzie, S. C.; Morrison, A. F.; Nanda, K. D.; Plasser, F.; Rehn, D. R.; Vidal, M. L.; You, Z.-Q.; Zhu, Y.; Alam, B.; Albrecht, B. J.; Aldossary, A.; Alguire, E.; Andersen, J. H.; Athavale, V.; Barton, D.; Begam, K.; Behn, A.; Bellonzi, N.; Bernard, Y. A.; Berquist, E. J.; Burton, H. G. A.; Carreras, A.; Carter-Fenk, K.; Chakraborty, R.; Chien, A. D.; Closser, K. D.; Cofer-Shabica, V.; Dasgupta, S.; Wergifosse, M. d.; Deng, J.; Diedenhofen, M.; Do, H.; Ehlert, S.; Fang, P.-T.; Fatehi, S.; Feng, Q.; Friedhoff, T.; Gayvert, J.; Ge, Q.; Gidofalvi, G.; Goldey, M.; Gomes, J.; González-Espinoza, C. E.; Gulania, S.; Gunina, A. O.; Hanson-Heine, M. W. D.; Harbach, P. H. P.; Hauser, A.; Herbst, M. F.; Vera, M. H.; Hodecker, M.; Holden, Z. C.; Houck, S.; Huang, X.; Hui, K.; Huynh, B. C.; Ivanov, M.; Jász, A.; Ji, H.; Jiang, H.; Kaduk, B.; Kähler, S.; Khistyaev, K.; Kim, J.; Kis, G.; Klunzinger, P.; Koczor-Benda, Z.; Koh, J. H.; Kosenkov, D.; Koulias, L.; Kowalczyk, T.; Krauter, C. M.; Kue, K.; Kunitsa, A.; Kus, T.; Ladjánszki, I.; Landau, A.; Lawler, K. V.; Lefrancois, D.; Lehtola, S.; Li, R. R.; Li, Y.-P.; Liang, J.; Liebenthal, M.; Lin, H.-H.; Lin, Y.-S.; Liu, F.; Liu, K.-Y.; Loipersberger, M.; Luenser, A.; Manjanath, A.; Manohar, P.; Mansoor, E.; Manzer, S. F.; Mao, S.-P.; Marenich, A. V.; Markovich, T.; Mason, S.; Maurer, S. A.; McLaughlin, P. F.; Menger, M. F. S. J.; Mewes, J.-M.; Mewes, S. A.; Morgante, P.; Mullinax, J. W.; Oosterbaan, K. J.; Paran, G.; Paul, A. C.; Paul, S. K.; Pavosević, F.; Pei, Z.; Prager, S.; Proynov, E. I.; Rák, A.; Ramos-Cordoba, E.; Rana, B.; Rask, A. E.; Rettig, A.; Richard, R. M.; Rob, F.; Rossomme, E.; Scheele, T.; Scheurer, M.; Schneider, M.; Sergueev, N.; Sharada, S. M.; Skomorowski, W.; Small, D. W.; Stein, C. I.; Su, Y.-C.; Sundstrom, E. J.; Tao, Z.; Thirman, J.; Tornai, G. J.; Tsuchimochi, T.; Tubman, N. M.; Veccham, S. P.; Vydrov, O.; Wenzel, J.; Witte, J.; Yamada, A.; Yao, K.; Yeganeh, S.; Yost, S. R.; Zech, A.; Zhang, I. Y.; Zhang, X.; Zhang, Y.; Zuev, D.; Aspuru-Guzik, A.; Bell, A. T.; Besley, N. A.; Bravaya, K. B.; Brooks, B. R.; Casanova, D.; Chai, J.-D.; Coriani, S.; Cramer, C. J.; Cserey, G.; DePrince, I. A. E.; DiStasioJr, R. A.; Dreuw, A.; Dunietz, B. D.; Furlani, T. R.; GoddardIII, W. A.; Hammes-Schiffer, S.; Head-Gordon, T.; Hehre, W. J.; Hsu, C.-P.; Jagau, T.-C.; Jung, Y.; Klamt, A.; Kong, J.; Lambrecht, D. S.; Liang, W.; Mayhall, N. J.; McCurdy, C. W.; Neaton, J. B.; Ochsenfeld, C.; Parkhill, J. A.; Peverati, R.; Rassolov, V. A.; Shao, Y.; Slipchenko, L. V.; Stauch, T.; Steele, R. P.; Subotnik, J. E.; Thom, A. J. W.; Tkatchenko, A.; Truhlar, D. G.; Voorhis, T. V.; Wesolowski, T. A.; Whaley, K. B.; WoodcockIII, H. L.; Zimmerman, P. M.; Faraji, S.; Gill, P. M. W.; Head-Gordon, M.; Herbert, J. M.; Krylov, A. I. Software for the frontiers of quantum chemistry: An overview of developments in the Q-Chem 5 package. J. Chem. Phys. 2021, 155, 084801.

(118) Sun, Q.; Zhang, X.; Banerjee, S.; Bao, P.; Barbry, M.; Blunt, N. S.; Bogdanov, N. A.; Booth, G. H.; Chen, J.; Cui, Z.-H.; Eriksen, J. J.; Gao, Y.; Guo, S.; Hermann, J.; Hermes, M. R.; Koh, K.; Koval, P.; Lehtola, S.; Li, Z.; Liu, J.; Mardirossian, N.; McClain, J. D.; Motta, M.; Mussard, B.; Pham, H. Q.; Pulkin, A.; Purwanto, W.; Robinson, P. J.; Ronca, E.; Sayfutyarova, E. R.; Scheurer, M.; Schurkus, H. F.; Smith, J. E. T.; Sun, C.; Sun, S.-N.; Upadhyay, S.; Wagner, L. K.; Wang, X.; White, A. F.; Whitfield, J. D.; Williamson, M. J.; Wouters, S.; Yang, J.; Yu, J. M.; Zhu, T.; Berkelbach, T. C.; Sharma, S.; Sokolov, A. Y.; Chan, G. K.-L. Recent developments in the PySCF program package. *J. Chem. Phys.* 2020, 153, 024109.

- (119) Loos, P.-F.; Scemama, A.; Blondel, A.; Garniron, Y.; Caffarel, M.; Jacquemin, D. A Mountaineering Strategy to Excited States: Highly Accurate Reference Energies and Benchmarks. *J. Chem. Theory Comput.* **2018**, *14*, 4360–4379.
- (120) Mazin, I. M.; Sokolov, A. Y. Multireference Algebraic Diagrammatic Construction Theory for Excited States: Extended Second-Order Implementation and Benchmark. *J. Chem. Theory Comput.* **2021**, *17*, 6152–6165.
- (121) Werner, H.-J.; Meyer, W. A quadratically convergent multiconfiguration—self-consistent field method with simultaneous optimization of orbitals and CI coefficients. *J. Chem. Phys.* **1980**, 73, 2342–2356.

- (122) Werner, H.-J.; Meyer, W. A quadratically convergent MCSCF method for the simultaneous optimization of several states. *J. Chem. Phys.* **1981**, *74*, 5794–5801.
- (123) Knowles, P. J.; Werner, H.-J. An efficient second-order MC SCF method for long configuration expansions. *Chem. Phys. Lett.* **1985**, *115*, 259–267.
- (124) Dyall, K. G. The choice of a zeroth-order Hamiltonian for second-order perturbation theory with a complete active space self-consistent-field reference function. *J. Chem. Phys.* **1995**, *102*, 4909–4918
- (125) Wolinski, K.; Sellers, H. L.; Pulay, P. Consistent generalization of the Møller-Plesset partitioning to open-shell and multiconfigurational SCF reference states in many-body perturbation theory. *Chem. Phys. Lett.* **1987**, *140*, 225–231.
- (126) Hirao, K. Multireference Møller—Plesset method. Chem. Phys. Lett. 1992, 190, 374-380.
- (127) Werner, H.-J. Third-order multireference perturbation theory. The CASPT3 method. *Mol. Phys.* **1996**, *89*, 645–661.
- (128) Finley, J.; Malmqvist, P.-Å.; Roos, B. O.; Serrano-Andrés, L. The multi-state CASPT2 method. *Chem. Phys. Lett.* **1998**, 288, 299–306.
- (129) Andersson, K.; Malmqvist, P. Å.; Roos, B. O.; Sadlej, A. J.; Wolinski, K. Second-order perturbation theory with a CASSCF reference function. *J. Chem. Phys.* **1990**, *94*, 5483–5488.
- (130) Andersson, K.; Malmqvist, P.-Å.; Roos, B. O. Second-order perturbation theory with a complete active space self-consistent field reference function. *J. Chem. Phys.* **1992**, *96*, 1218–1226.
- (131) Angeli, C.; Cimiraglia, R.; Evangelisti, S.; Leininger, T.; Malrieu, J.-P. P. Introduction of n-electron valence states for multireference perturbation theory. *J. Chem. Phys.* **2001**, *114*, 10252–10264.
- (132) Angeli, C.; Cimiraglia, R.; Malrieu, J.-P. P. N-electron valence state perturbation theory: a fast implementation of the strongly contracted variant. *Chem. Phys. Lett.* **2001**, *350*, 297–305.
- (133) Angeli, C.; Borini, S.; Cestari, M.; Cimiraglia, R. A quasidegenerate formulation of the second order n-electron valence state perturbation theory approach. *J. Chem. Phys.* **2004**, *121*, 4043–4049.
- (134) Buth, C.; Birkenheuer, U.; Albrecht, M.; Fulde, P. Ab initio Green's function formalism for band structures. *Phys. Rev. B* **2005**, *72*, 195107.
- (135) Buth, C. Quasiparticle band structure of infinite hydrogen fluoride and hydrogen chloride chains. *J. Chem. Phys.* **2006**, *125*, 154707.
- (136) Bezugly, V.; Albrecht, M.; Birkenheuer, U. Comparison of three quantum chemical *ab initio* methods for band structure calculations: the hydrogen fluoride chain. *J. Phys. Conf. Ser.* **2008**, *117*, 012006.
- (137) McClain, J.; Sun, Q.; Chan, G. K. L.; Berkelbach, T. C. Gaussian-Based Coupled-Cluster Theory for the Ground-State and Band Structure of Solids. *J. Chem. Theory Comput.* **2017**, *13*, 1209–1218
- (138) Sun, Q.; Berkelbach, T. C.; McClain, J. D.; Chan, G. K.-L. Gaussian and plane-wave mixed density fitting for periodic systems. *J. Chem. Phys.* **2017**, *147*, 164119.
- (139) Cederbaum, L. S.; Domcke, W.; Schirmer, J. Many-body theory of core holes. *Phys. Rev. A* 1980, 22, 206–222.
- (140) Barth, A.; Cederbaum, L. S. Many-body theory of core-valence excitations. *Phys. Rev. A* **1981**, 23, 1038–1061.
- (141) Köppel, H.; Gadea, F.; Klatt, G.; Schirmer, J.; Cederbaum, L. Multistate vibronic coupling effects in the K-shell excitation spectrum of ethylene: Symmetry breaking and core-hole localization. *J. Chem. Phys.* **1997**, *106*, 4415–4429.
- (142) Trofimov, A. B.; Moskovskaya, T. E.; Gromov, E. V.; Vitkovskaya, N. M.; Schirmer, J. Core-level electronic spectra in ADC(2) approximation for polarization propagator: Carbon monoxide and nitrogen molecules. *J. Struct. Chem.* **2000**, *41*, 483–494.
- (143) Wenzel, J.; Wormit, M.; Dreuw, A. Calculating X-ray Absorption Spectra of Open-Shell Molecules with the Unrestricted

- Algebraic-Diagrammatic Construction Scheme for the Polarization Propagator. J. Chem. Theory Comput. 2014, 10, 4583–4598.
- (144) Wenzel, J.; Wormit, M.; Dreuw, A. Calculating core-level excitations and X-ray absorption spectra of medium-sized closed-shell molecules with the algebraic-diagrammatic construction scheme for the polarization propagator. *J. Comput. Chem.* **2014**, *35*, 1900–1915.
- (145) Wenzel, J.; Holzer, A.; Wormit, M.; Dreuw, A. Analysis and comparison of CVS-ADC approaches up to third order for the calculation of core-excited states. *J. Chem. Phys.* **2015**, *142*, 214104.
- (146) Coriani, S.; Koch, H. Communication: X-ray absorption spectra and core-ionization potentials within a core-valence separated coupled cluster framework. *J. Chem. Phys.* **2015**, *143*, 181103.
- (147) Vidal, M. L.; Feng, X.; Epifanovsky, E.; Krylov, A. I.; Coriani, S. New and Efficient Equation-of-Motion Coupled-Cluster Framework for Core-Excited and Core-Ionized States. *J. Chem. Theory Comput.* **2019**, *15*, 3117–3133.
- (148) Liu, J.; Matthews, D. A.; Coriani, S.; Cheng, L. Benchmark Calculations of K-Edge Ionization Energies for First-Row Elements Using Scalar-Relativistic Core—Valence-Separated Equation-of-Motion Coupled-Cluster Methods. J. Chem. Theory Comput. 2019, 15, 1642—1651.
- (149) Helmich-Paris, B. Simulating X-ray absorption spectra with complete active space self-consistent field linear response methods. *Int. J. Quantum Chem.* **2021**, *121*, No. e26559.
- (150) Thielen, S. M.; Hodecker, M.; Piazolo, J.; Rehn, D. R.; Dreuw, A. Unitary coupled-cluster approach for the calculation of core-excited states and x-ray absorption spectra. *J. Chem. Phys.* **2021**, *154*, 154108.
- (151) Dobrodey, N. V.; Cederbaum, L. S.; Tarantelli, F. Local and nonlocal effects in the core ionization of metal-molecule adsorbates and cluster systems. *Phys. Rev. B* **2000**, *61*, 7336–7339.
- (152) Dobrodey, N. V.; Streltsov, A. I.; Cederbaum, L. S. Coreionized states and spectra of Be and Mg dimers. *Phys. Rev. A* **2002**, *65*, 022501.
- (153) Dobrodey, N. V.; Streltsov, A. I.; Cederbaum, L. S.; Villani, C.; Tarantelli, F. Foreign and native coordination effects in core-level spectra of mixed Be-Mg clusters. *J. Chem. Phys.* **2002**, *117*, 3533–3526
- (154) Dobrodey, N. V.; Streltsov, A. I.; Cederbaum, L. S.; Villani, C.; Tarantelli, F. Strong charge-transfer effects in the Mg 2p⁻¹ core-level spectrum of MgB₂. *Phys. Rev. B* **2002**, *66*, 165103.
- (155) Plekan, O.; Feyer, V.; Richter, R.; Coreno, M.; de Simone, M.; Prince, K.C.; Trofimov, A.B.; Gromov, E.V.; Zaytseva, I.L.; Schirmer, J. A theoretical and experimental study of the near edge X-ray absorption fine structure (NEXAFS) and X-ray photoelectron spectra (XPS) of nucleobases: Thymine and adenine. *Chem. Phys.* **2008**, 347, 360–375.
- (156) Zhu, Q.; Wang, F.; Ivanova, E. Impact of ketone and amino on the inner shell of guanine. *J. Synchrotron Radiat.* **2009**, *16*, 545–552.
- (157) Trofimov, A. B.; Belogolova, A. M.; Serebrennikova, S. A.; Forbes, R.; Pratt, S. T.; Holland, D. M. P. An experimental and theoretical study of the C 1s ionization satellites in CH3I. *J. Chem. Phys.* **2019**, *150*, 224303.
- (158) Herbst, M. F.; Fransson, T. Quantifying the error of the corevalence separation approximation. *J. Chem. Phys.* **2020**, *153*, 054114.
- (159) Cannington, P.; Ham, N. S. He (I) and He (II) photoelectron spectra of glycine and related molecules. *J. Electron Spectrosc. Relat. Phenom.* 1983, 32, 139–151.
- (160) Kubala, D.; Regeta, K.; Janecková, R.; Fedor, J.; Grimme, S.; Hansen, A.; Nesvadba, P.; Allan, M. The electronic structure of TEMPO, its cation and anion. *Mol. Phys.* **2013**, *111*, 2033–2040.
- (161) Banna, M. S.; Frost, D. C.; McDowell, C. A.; Noodleman, L.; Wallbank, B. A study of the core electron binding energies of ozone by x-ray photoelectron spectroscopy and the $X\alpha$ scattered wave method. *Chem. Phys. Lett.* **1977**, *49*, 213–217.
- (162) Hayes, E. F.; Siu, A. K. Q. Electronic structure of the open forms of three-membered rings. *J. Am. Chem. Soc.* **1971**, 93, 2090–2091.

- (163) Hay, P. J.; Dunning, T. H.; Goddard, W. A. Configuration interaction studies of O_3 and O_3^+ . Ground and excited states. *J. Chem. Phys.* **1975**, *62*, 3912–3924.
- (164) Laidig, W. D.; Schaefer, H. F. Large multiconfiguration self-consistent-field wave functions for the ozone molecule. *J. Chem. Phys.* **1981**, *74*, 3411–3414.
- (165) Schmidt, M. W.; Gordon, M. S. The construction and interpretation of MCSCF wavefunctions. *Annu. Rev. Phys. Chem.* **1998**, *49*, 233–266.
- (166) Kalemos, A.; Mavridis, A. Electronic structure and bonding of ozone. *J. Chem. Phys.* **2008**, 129, 054312.
- (167) Musiał, M.; Kucharski, S. A.; Zerzucha, P.; Kuś, T.; Bartlett, R. J. Excited and ionized states of the ozone molecule with full triples coupled cluster methods. *J. Chem. Phys.* **2009**, *131*, 194104.
- (168) Miliordos, E.; Ruedenberg, K.; Xantheas, S. S. Unusual Inorganic Biradicals: A Theoretical Analysis. *Angew. Chem., Int. Ed.* **2013**, *52*, 5736–5739.
- (169) Takeshita, T. Y.; Lindquist, B. A.; Dunning, T. H. Insights into the Electronic Structure of Ozone and Sulfur Dioxide from Generalized Valence Bond Theory: Bonding in O₃ and SO₂. *J. Phys. Chem. A* **2015**, *119*, 7683–7694.
- (170) Melania Oana, C.; Krylov, A. I. Dyson orbitals for ionization from the ground and electronically excited states within equation-of-motion coupled-cluster formalism: Theory, implementation, and examples. J. Chem. Phys. 2007, 127, 234106.
- (171) Ortiz, J. V. Dyson-orbital concepts for description of electrons in molecules. *J. Chem. Phys.* **2020**, *153*, 070902.
- (172) Plasser, F.; Wormit, M.; Dreuw, A. New tools for the systematic analysis and visualization of electronic excitations. I. Formalism. *J. Chem. Phys.* **2014**, *141*, 024106.
- (173) Schutz, M.; Werner, H.-J. Low-order scaling local electron correlation methods. IV. Linear scaling local coupled-cluster (LCCSD). *J. Chem. Phys.* **2001**, *114*, 661–681.
- (174) Werner, H.-J.; Manby, F. R.; Knowles, P. J. Fast linear scaling second-order Møller-Plesset perturbation theory (MP2) using local and density fitting approximations. *J. Chem. Phys.* **2003**, *118*, 8149–8160.
- (175) Riplinger, C.; Neese, F. An efficient and near linear scaling pair natural orbital based local coupled cluster method. *J. Chem. Phys.* **2013**, *138*, 034106–034106–18.
- (176) Taube, A. G.; Bartlett, R. J. Frozen Natural Orbitals: Systematic Basis Set Truncation for Coupled-Cluster Theory. *Collect. Czech. Chem. Commun.* **2005**, *70*, 837–850.
- (177) Mester, D.; Nagy, P. R.; Kállay, M. Reduced-cost second-order algebraic-diagrammatic construction method for excitation energies and transition moments. *J. Chem. Phys.* **2018**, *148*, 094111.
- (178) Hohenstein, E. G.; Parrish, R. M.; Martinez, T. J. Tensor hypercontraction density fitting. I. Quartic scaling second- and third-order Møller-Plesset perturbation theory. *J. Chem. Phys.* **2012**, *137*, 044103–044103–10.
- (179) Parrish, R. M.; Hohenstein, E. G.; Martinez, T. J.; Sherrill, C. D. Tensor hypercontraction. II. Least-squares renormalization. *J. Chem. Phys.* **2012**, *137*, 224106–224106–11.
- (180) Hohenstein, E. G.; Parrish, R. M.; Sherrill, C. D.; Martinez, T. J. Communication: Tensor hypercontraction. III. Least-squares tensor hypercontraction for the determination of correlated wavefunctions. *J. Chem. Phys.* **2012**, *137*, 221101.
- (181) Scheurer, M.; Herbst, M. F.; Reinholdt, P.; Olsen, J. M. H.; Dreuw, A.; Kongsted, J. Polarizable Embedding Combined with the Algebraic Diagrammatic Construction: Tackling Excited States in Biomolecular Systems. J. Chem. Theory Comput. 2018, 14, 4870–4883
- (182) Ohio Supercomputer Center; 1987; http://osc.edu/ark:/19495/f5s1ph73.